UNIVERSIDADE FEDERAL DE MATO GROSSO
CÂMPUS UNIVERSITÁRIO DE SINOP
INSTITUTO DE CIÊNCIAS NATURAIS, HUMANAS E SOCIAIS
PROGRAMA DE PÓS-GRADUAÇÃO EM CIÊNCIAS AMBIENTAIS

João Lucas Della Silva

AMAZONIAN FLORISTICS AND ANTHROPIZATION ASSESSMENT THROUGH MULTI AND HYPERSPECTRAL REMOTE SENSING

SINOP
MATO GROSSO - BRASIL
2022

UNIVERSIDADE FEDERAL DE MATO GROSSO
CÂMPUS UNIVERSITÁRIO DE SINOP
INSTITUTO DE CIÊNCIAS NATURAIS, HUMANAS E SOCIAIS
PROGRAMA DE PÓS-GRADUAÇÃO EM CIÊNCIAS AMBIENTAIS

João Lucas Della Silva

AMAZONIAN FLORISTICS AND ANTHROPIZATION ASSESSMENT THROUGH MULTI AND HYPERSPECTRAL REMOTE SENSING

Advisor: Prof. Dr. Carlos Antonio da Silva Junior

Master thesis presented to Programa de Pós-Graduação em Ciências Ambientais of Universidade Federal de Mato Grosso, Sinop University Campus, in the Biodiversity and Bioprospecting concentration area, as part of the requirements for obtaining the title of Master in Environmental Sciences.

Research line: Natural Resources.

SINOP
MATO GROSSO - BRASIL
2022

CATALOGUE CARD

Dados Internacionais de Catalogação na Fonte.

S586a Silva, João Lucas Della.
Amazonian floristics and anthropization through multi and hyperspectral remote sensing / João Lucas Della Silva. -- 2022
xii, 83 f. : il. color. ; 30 cm.

Orientador: Carlos Antonio da Silva Junior.
Dissertação (mestrado) - Universidade Federal de Mato Grosso, Instituto de Ciências Naturais, Humanas e Sociais, Programa de Pós-Graduação em Ciências Ambientais, Sinop, 2022.
Inclui bibliografia.

1. Sensoriamento remoto do ambiente. 2. sensoriamento remoto hiperespectral. 3. índices de vegetação. 4. espécies florestais amazônicas. 5. dinâmica do carbono. I. Título.

Ficha catalográfica elaborada automaticamente de acordo com os dados fornecidos pelo(a) autor(a).

APPROVAL SHEET

MINISTÉRIO DA EDUCAÇÃO
UNIVERSIDADE FEDERAL DE MATO GROSSO
PRÓ-REITORIA DE ENSINO DE PÓS-GRADUAÇÃO
PROGRAMA DE PÓS-GRADUAÇÃO EM [NOME DO PPG]

FOLHA DE APROVAÇÃO

TÍTULO: Amazonian floristics and anthropization assessment through multi and hyperspectral remote sensing

AUTOR (A): MESTRANDO (A) **João Lucas Della Silva**

Dissertação defendida e aprovada em **25/01/2022.**

COMPOSIÇÃO DA BANCA EXAMINADORA

1. Doutor(a) Carlos Antonio da Silva Junior (Presidente Banca / Orientador)
INSTITUIÇÃO: Universidade do Estado de Mato Grosso
2. Doutor(a) Paulo Eduardo Teodoro (Examinador Externo)
INSTITUIÇÃO: Universidade Federal de Mato Grosso do Sul
3. Doutor(a) Mendelson Guerreiro de Lima (Examinador Externo)
INSTITUIÇÃO: Universidade do Estado de Mato Grosso
4. Doutor(a) Larissa Pereira Ribeiro Teodoro (Examinador Suplente)
INSTITUIÇÃO: Universidade Federal de Mato Grosso do Sul
5. Doutor(a) Guilherme Fernando Capristo Silva (Examinador Suplente)
INSTITUIÇÃO: PNPD - Programa Nacional de Pós-doutorado - UFMT

SINOP, 25/01/2022.

Documento assinado eletronicamente por **Paulo Eduardo Teodoro**, **Usuário Externo**, em 25/01/2022, às 12:27, conforme horário oficial de Brasília, com fundamento no art. 6º, § 1º, do Decreto nº 8.539, de 8 de outubro de 2015.

Documento assinado eletronicamente por **Carlos Antonio da Silva Junior**, **Usuário Externo**, em 25/01/2022, às 12:31, conforme horário oficial de Brasília, com fundamento no art. 6º, § 1º, do Decreto nº 8.539, de 8 de outubro de 2015.

Documento assinado eletronicamente por **Mendelson Guerreiro de Lima**, **Usuário Externo**, em 26/01/2022, às 10:27, conforme horário oficial de Brasília, com fundamento no art. 6º, § 1º, do Decreto nº 8.539, de 8 de outubro de 2015.

A autenticidade deste documento pode ser conferida no site http://sei.ufmt.br/sei/controlador_externo.php?acao=documento_conferir&id_orgao_acesso_externo=0, informando o código verificador **4339390** e o código CRC **82B71D22**.

Referência: Processo nº 23108.001702/2022-21 SEI nº 4339390

ACKNOWLEDGEMENTS

I am grateful to God, who gave me the gift of life and makes it an incredible experience, and makes me fulfilled and grateful to many people.

I am grateful to my parents, Olandina and João Batista, firstly to give me education, what puts me writing this work and acknowledgements, especially in English. You are my daily inspiration to be a good professional, good man and a good son for you both. And thank you so much for making my journey accompanied by a sister and a brother. About them, I'm thankful for you, Giovana and Danilo, for being an important part of my life. All of my respect, brotherly love and support I'll give you, as long as I live.

I am hugely thankful for my girl, Bianca, who has been by my side since she met me, and strengthens me in each challenge and presents me with a new me, fulfilled and eager to continue improving myself.

I am grateful to Carlos, advisor and friend, who gave support and aid to make this learning and projects pleasant, and did each step a new and important apprenticeship. I'm really thankful for each lab colleague, especially Fernando, for helping me on research and be good friends and companions.

I am really grateful to Universidade do Estado de Mato Grosso – UNEMAT for being important part of my life, since I wasn't even born. And I'm thankful for Universidade Federal de Mato Grosso – UFMT for sheltering me by PPGCAM. Beyond universities, I'm thankful for each professor in my master's formation, you were of unparalleled importance to make this happen.

I thank professors Dr. Luciano Shozo Shiratsuchi (Louisiana State University) and Dr. Mendelson Guerreiro de Lima (University of Mato Grosso State), for contributing with the spectroradiometric data acquisition, and professor Dr. Marcos Rafael Nanni with the airborne data generation.

I'm thankful to Universidade de Maringá – UEM for making the AisaFENIX sensor available and to Embrapa Agrossilvopastoril which provided FieldSpec 4 Hi-Res. Finally, I'm grateful to Coordenação de Aperfeiçoamento de Pessoal Nível Superior – CAPES, for the scholarship.

RESUMO EM LÍNGUA VERNÁCULA

A gestão dos recursos florestais com viés ecológico passa pela caracterização fitossociológica, e se torna fundamental quando observadas as espécies de plantas da Amazônia. Dentre os métodos de inventariação florestal, o sensoriamento remoto aplica-se a pesquisas e monitoramento destes recursos com tecnologias baseadas na espectrometria. Tão importante quanto, a análise da dinâmica de uso e ocupação do solo de áreas nativas são associadas à gestão de recursos naturais e o monitoramento de áreas antropizadas. A aplicabilidade de tecnologias desta ciência é verificada neste trabalho, inicialmente na distinção entre espécies florestais por meio da espectrorradiometria e posteriormente na validação do modelo hiperespectral de estimativa de capacidade de absorção de dióxido de carbono em dados orbitais multiespectrais. Na primeira verificação, dados baseados no espectrorradiômetro FieldSpec® 4 Hi-Res relativos a quatro espécies de árvores amazônicas (i. e. *Bertholletia excelsa*, *Cedrela fissilis*, *Euterpe Oleracea* e *Schizolobium parahyba*) foram submetidas à análise de Componentes Principais (PC) e a Análise Discriminatória, que permearam a distinção das assinaturas espectrais e de modelos que representam estas assinaturas (RID, bandas representativas e índices de vegetação). O êxito na diferenciação por meio deste método é observado com a variabilidade dos dados sendo descritos por PC1 superior a 99% com os três modelos de redução de dimensionalidade aplicados. Observando-se os resultados da análise de PC aplicada aos índices espectrais, o critério de Singh permitiu verificar que os índices NPCI e CARI2 foram majoritariamente responsáveis pela diferenciação das assinaturas espectrais das espécies avaliadas, que são índices associados à interação da clorofila com a radiação solar no espectro visível. O segundo estudo trata da comparação de resultados do índice CO_2Flux entre o sensor hiperespectral AisaFENIX e os sensores orbitais multiespectrais OLI/Landsat-8, MSI/Sentinel-2 e PlanetScope, com este índice aplicado de forma adaptada. Este estudo foi realizado sobre uma cena com áreas de floresta nativa, pastagem e solo exposto na cidade de Alta Floresta, na Amazônia meridional. Por meio da análise de variância, observou-se que o índice CO_2Flux é pouco relacionado ao índice PRI, um dos índices base para o CO_2Flux. Além disso, os resultados sugerem que o MSI/Sentinel-2 é estatisticamente semelhante ao sensor AisaFENIX nas áreas antropizadas. Finalmente, a variabilidade temporal destes resultados pode melhorar estas conclusões, tendo em vista a relação entre conteúdo de água no dossel com os índices de base do CO_2Flux.

Palavras-chave: sensoriamento remoto do ambiente, sensoriamento remoto hiperespectral, índices de vegetação, espécies florestais amazônicas, dinâmica do carbono.

ABSTRACT

The management of forest resources with an ecological bias involves phytosociological characterization, and becomes fundamental when observing the plant species of the Amazon. Among the methods of forest inventory, remote sensing applies to research and monitoring of these resources with technologies based on spectrometry. Just as important, the analysis of the dynamics of land use and occupation of native areas are associated with the management of natural resources and the monitoring of anthropized areas. The applicability of this science's technologies is verified in this work, initially in the distinction between forest species by means of spectroradiometry and later in the validation of the hyperspectral model for estimating carbon dioxide absorption capacity in multispectral orbital data. In the first verification, FieldSpec® 4 Hi-Res spectroradiometer-based data for four Amazonian tree species (i. e. *Bertholletia excelsa, Cedrela fissilis, Euterpe Oleracea* and *Schizolobium parahyba*) were subjected to Principal Component (PC) analysis and Discriminant Analysis, which permeated the distinction of spectral signatures and models representing these signatures (RID, representative bands and vegetation indices). The success in differentiation by this method is observed with the variability of the data being described by PC1 greater than 99% with the three dimensionality reduction models applied. Observing the PC results applied to the spectral indices, Singh's criterion allowed to verify that the NPCI and CARI2 indices were mostly responsible for the differentiation of the spectral signatures of the evaluated species, which are indices associated with the interaction of chlorophyll with solar radiation in the visible spectrum. The second study deals with the comparison of CO_2Flux index results between the hyperspectral sensor AisaFENIX and the multispectral orbital sensors OLI/Landsat-8, MSI/Sentinel-2 and PlanetScope, with this index applied in an adapted way. This study was carried out over a scene with native forest, pasture and bare soil areas in the city of Alta Floresta, in southern Amazonia. Through analysis of variance, it was observed that the CO_2Flux index is poorly related to the PRI index, one of the base indices for CO_2Flux. Furthermore, the results suggest that MSI/Sentinel-2 are statistically similar to the AisaFENIX sensor in the anthropized areas. Finally, the temporal variability of these results may improve these conclusions, given the relationship between water content in the canopy to the base indices of the CO_2Flux.

Keywords: remote sensing of environment, hyperspectral remote sensing, vegetation indices, Amazonian Forest species, carbon dynamics.

LISTS

LIST OF ABBREVIATIONS AND ACRONYMS

CARI2 – Chlorophyll Absorption Ratio Index

CO_2Flux – Carbon dioxide flux

EVI – Enhanced Vegetation Index

fAPAR – Fraction of photosynthetically active radiation absorbed by green biomass

GLI – Green Leaf Index

GNDVI – Green Normalized Difference Vegetation Index

HSI - Hyperspectral Image

LCI – Leaf Chlorophyll Index

LUE – Light Use Efficiency

LULC – Land Use and Land Cover

LWCI – Leaf Water Content Index

MSI – Multispectral Imager

NDVI – Normalized Difference Vegetation Index

NPCI – Normalized Pigment Chlorophyll Index

OLI – Operational Land Imager

OSAVI – Optimized Soil Adjusted Vegetation Index

PC – Principal Component

PRI – Photochemical Reflectance Index

RID – Reflectance Inflection Difference

ROI – Region of Interest

SAVI – Soil Adjusted Vegetation Index

TVI – Transformed Vegetation Index

LIST OF ILLUSTRATIONS/FIGURES

CHAPTER I.

CHAPTER II.

LIST OF TABLES

CHAPTER I.

CHAPTER II.

SUMMARY

GENERAL INTRODUCTION OF THESIS

The characterization of the floristic composition is essential in forestry studies, although its execution is based on methods with a high technical cost, which in turn are based on statistical analysis with outdated data (OUÉDRAOGO et al., 2011) or in chaotic methods (PEREIRA; ALVES, 2007), which can give a significant error. Furthermore, it is a slow process based on morphological and anatomical observations of leaves, floral structures and other trees characteristics (GAUI et al., 2019).

The characterization of the floristic composition is essential in forestry studies, although its execution is based on methods with a high technical cost, which in turn are based on statistical analysis with outdated data (OUÉDRAOGO et al., 2011) or in chaotic methods (PEREIRA; ALVES, 2007), which can give a significant error. Furthermore, it is a slow process based on morphological and anatomical observations of leaves, floral structures and other trees characteristics (GAUI et al., 2019).

Several plant species are distinguished by their characteristics, such as floral structures. To identify and locate certain species, the plant must be in bloom to allow the eventual botanical research that is being carried out (VENTER; WITKOWSKI, 2019). In places with high diversity, this process of floristic characterization is even more complex whereas many species remain unknown and some have a very restricted flowering period during the year, which affects the process of locating them (ARAUJO, 2006).

This lack of knowledge regarding diversity is accentuated when native forest species in the Amazon biome are assessed (DE ASSIS et al., 2017). Combining this to the selective exploration of the biome, more effective and faster techniques are required for trees identification and localization, as well as recognizing physical and chemical attributes, distinct for each plant variety (HOPE, 2019).

In a broad perspective, the native forests dynamics assessment in Brazil are based on the System of Permanent Parcels (in Portuguese, SisPP) and Forest Dynamics Monitoring Network (PP Networks) that bring together the institutions datasets of the forestry sector, in terms of dynamics of growth and forestry production, which has as a product the implementation of continuous forest inventories (SOUZA, 2013). Vegetation assessment methods are generally based on systematized assessments and in rare scenarios censuses are performed (DE FREITAS; MAGALHÃES, 2012).

Among the forest inventory methods, remote sensing is applicable, which is characterized by the acquisition of data on objects without physical contact with them, using sensor systems for data generation and software for data processing (LILLESAND; KIEFER, 1994).

Remote sensors are classified according to their spectral resolution, and are basically distinguished into two classes, these being multispectral and hyperspectral sensors. Those classes imply the type of data obtained, and also defines the applicability and relevancy (PONZONI; SHIMABUKURO, 2009).

Generally, studies of diversity or floristic composition of natural environments are based on multispectral data (dozens of electromagnetic bands), which are based on orbital sensor systems and are generally freely accessible. Characteristics such as texture, viridity and collateral information are the basis for classification and analysis of images for the purpose of determining (only) the diversity of plant species (ADAMS et al., 2019; MURO et al., 2016; TADDEO; DRONOVA; HARRIS, 2021). This type of database is very efficient in applications with large areas, such as defining the boundaries among biomes (SILVA JUNIOR et al., 2019a).

From the perspective of hyperspectral remote sensing (based on hundreds of electromagnetic bands), sensors are divided into hyperspectral imagers (data represented as images), and non-imagers (data represented as spectral signatures, digits or images) (DPI/INPE, 2006), where non-imaging sensors are more promising in plant applications, since for this research level the metabolic and biophysical characteristics of the individual are analyzed in more detail (JAMES B. CAMPBELL, 2011; WEST et al., 2010).

Hyperspectral sensor data model the remote sensing of the environment, where the various possible targets are represented by the fingerprint (or spectral signature) relative to that target. The spectral signature is graphically represented, where the curve is based on the relation between electromagnetic wavelength and reflectance (MENESES et al., 2012).

Plants leaves have complex information from organic compounds and can exhibit distinct spectral characteristics when studied in the infrared energy range. Thus, modes of functional vibrations of various molecular groups produce characteristic spectral absorption that can generate a thorough fingerprint (SILVERSTEIN et al., 2015).

Hyperspectral sensors allow detailed and reliable characterization of the spatial variability of a given study area, and also of certain species, as an example, stage of development, nutritional status and other countless possibilities. As they operate in

hundreds of contiguous and narrow spectral bands, presenting a very high spectral resolution (non-imaging sensors like FieldSpec4®) and spatial resolution (when using imaging sensors, like the Specim® AisaFENIX sensor) the evaluation, identification, classification and eventual localization is only possible through the spectral signature or response that each object presents (VANE; GOETZ, 1993).

In addition, computational treatments to remote data, such as the use of vegetation indices and digital classifiers, join this kind of data and information regarding biophysical parameters of plants, and consequently allow the distinction and characterization of plant targets (FORMAGGIO; SANCHES, 2017).

The structuring of the spectral signature of plant species is the basis for defining an input parameter for many applications and analyzes based on spectroscopy of plants, and proves to be a very effective reference in distinguishing between species using various classification methods. Moreover, approaches with this bias are characterized by not necessarily destructive, and can be developed without the suppression of plants from the environment (KHDERY; YONES, 2020; LU et al., 2020; NIDAMANURI, 2020; VAIPHASA et al., 2007).

In addition to distinguishing among species, spectroscopy is applied in plants to distinguish among subspecies (GALVÃO; FORMAGGIO; TISOT, 2005; SILVA JUNIOR et al., 2018), detection of boron deficiency in eucalyptus (SILVA et al., 2019), heavy metal stress (YU; FANG; ZHAO, 2021) and water deficit (BONILLA, 2015; CRUSIOL et al., 2017; FIORIO et al., 2018). On chapter 1, were applied three downsizing data methods to spectral responses from Amazonian tree species, combined to Principal Component (PC) analysis and Cluster Analysis on species distinction.

Besides, remote sensing is applied on carbon balance characterization of a land cover type (SILVA JUNIOR et al., 2019b; SOUZA et al., 2021), and this quantity can be estimated by spectral indices. Rahman et al (2001) developed the atmospheric carbon dioxide absorption efficiency model for a given area, composed by two spectral indices of normalized difference, which are Normalized Difference Vegetation Index (ROUSE et al., 1974) and Photochemical Reflectance Index (GAMON; SERRANO; SURFUS, 1997).

Due to the dependence on a hyperspectral index, the applicability of this Rahman CO2 uptake model is spatially and spectrally limited (GAMON; SERRANO; SURFUS, 1997; INOUE et al., 2008). Nevertheless, the application of this model adapted to multispectral bases has proven to be functional and has been disseminated in research

into remote sensing of the environment with good results (CORREIA FILHO et al., 2021; DO NASCIMENTO LOPES et al., 2019; FERNANDEZ et al., 2021; SILVA JUNIOR et al., 2019b).

Apparently, this is due to a greater reliance of the estimated CO2 uptake value on the NDVI. Seeking to validate and expand the applicability of Rahman's model (2001) in the realm of multispectral orbital remote sensing, chapter 2 of this thesis will compare the results for this model in the same imaged area with data from the Specim® AisaFENIX hyperspectral sensor and the Landsat-8/OLI, Sentinel-2/MSI and PlanetScope multispectral orbital sensor systems. The study area is located in the southern Amazon, in the municipality of Alta Floresta - MT. It is worth noting that the area imaged has forest, exposed soil and pasture, allowing an extended and sturdy comparison of these three types of land use and land cover (LULC).

In this context, hyperspectral remote sensing techniques and multivariate statistics were applied to the distinction of plants of some species that make up the flora of an area of the Amazon biome, using the FieldSpec4® sensor, and data from the Specim® AisaFENIX sensor to validate the applicability of the model for estimating efficiency in atmospheric carbon uptake in the Amazon biome.

BIBLIOGRAFIC REFERENCES

ADAMS, Bryce T.; MATTHEWS, Stephen N.; PETERS, Matthew P.; PRASAD, Anantha; IVERSON, Louis R. Mapping floristic gradients of forest composition using an ordination-regression approach with landsat OLI and terrain data in the Central Hardwoods region. **Forest Ecology and Management**, *[S. l.]*, v. 434, n. December 2018, p. 87–98, 2019. DOI: 10.1016/j.foreco.2018.12.018. Disponível em: https://doi.org/10.1016/j.foreco.2018.12.018.

ARAUJO, Henrique José Borges De. Inventário florestal a 100% em pequenas áreas sob manejo florestal madeireiro. **Acta Amazonica**, *[S. l.]*, v. 36, n. 4, p. 447–464, 2006. DOI: 10.1590/s0044-59672006000400007. Disponível em: https://doi.org/10.1590/s0044-59672006000400007.

BONILLA, Magda Maria Zuleta. **Dados hiperespectrais na determinação do conteúdo relativo de água na folha em cana-de-açúcar**. 2015. Universidade de São Paulo, Piracicaba, 2015. DOI: 10.11606/D.11.2015.tde-28092015-105933. Disponível

em: https://www.teses.usp.br/teses/disponiveis/11/11152/tde-28092015-105933/en.php.

CORREIA FILHO, Washington Luiz Félix; SANTIAGO, Dimas de Barros; OLIVEIRA-JÚNIOR, José Francisco De; SILVA JUNIOR, Carlos Antonio Da; OLIVEIRA, Stella Rosane da Silva; SILVA, Elania Barros Da; TEODORO, Paulo Eduardo. Analysis of environmental degradation in Maceió-Alagoas, Brazil via orbital sensors: A proposal for landscape intervention based on urban afforestation. **Remote Sensing Applications: Society and Environment**, *[S. l.]*, v. 24, p. 100621, 2021. DOI: https://doi.org/10.1016/j.rsase.2021.100621. Disponível em: https://www.sciencedirect.com/science/article/pii/S2352938521001579.

CRUSIOL, L. G. T. et al. Sensoriamento remoto aplicado ao monitoramento do déficit hídrico na cultura da soja. *In*: EMBRAPA SOJA-ARTIGO EM ANAIS DE CONGRESSO (ALICE) 2017, **Anais** [...]. [s.l: s.n.]

DE ASSIS, Rafael Leandro; WITTMANN, Florian; LUIZE, Bruno Garcia; HAUGAASEN, Torbjørn. **Patterns of floristic diversity and composition in floodplain forests across four Southern Amazon river tributaries, BrazilFlora**, 2017. DOI: https://doi.org/10.1016/j.flora.2017.02.019. Disponível em: https://www.sciencedirect.com/science/article/pii/S0367253017331481.

DE FREITAS, Welington Kiffer; MAGALHÃES, Luís Mauro Sampaio. Métodos e Parâmetros para Estudo da Vegetação com Ênfase no Estrato Arbóreo. **Floresta e Ambiente**, [S. l.], v. 19, n. 4, p. 520–540, 2012. DOI: 10.4322/floram.2012.054.

DO NASCIMENTO LOPES, Elfany Reis; SOUSA, Jocy Ana Paixão De; SOUZA, José Carlos De; FILHO, José Luiz Albuquerque; LOURENÇO, Roberto Wagner. Spatial dynamics of Atlantic Forest fragments in a river basin. FLORESTA, *[S. l.]*, v. 50, n. 1, p. 1053, 2019. DOI: 10.5380/rf.v50i1.61076. Disponível em: https://doi.org/10.5380/rf.v50i1.61076.

DPI/INPE. **Manuais: Tutorial de Geoprocessamento**. 2006. Disponível em: http://www.dpi.inpe.br/spring/portugues/tutorial/index.html.

FERNANDEZ, Helena M.; GRANJA-MARTINS, Fernando M.; PEDRAS, Celestina M. G.; FERNANDES, Patrícia; ISIDORO, Jorge M. G. P. An Assessment of Forest Fires and CO2 Gross Primary Production from 1991 to 2019 in Mação (Portugal), **Sustainability**, 2021. DOI: 10.3390/su13115816.

FIORIO, Peterson Ricardo; COELHO, Rubens Duarte; BARROS, Pedro Paulo Silva; BONILLA, Magda Maria Zuleta; GADY, Ana Paula Barbosa. Comportamento Espectral De Folhas Da Cana-De-Açúcar Na Presença De Déficit Hídrico. **Irriga**, *[S.*

l.],v. 23, n. 3, p. 609–621, 2018. DOI: 10.15809/irriga.2018v23n3p609-621. Disponível em: https://200.145.140.50/index.php/irriga/article/view/2673/2421.

FORMAGGIO, Antonio Roberto; SANCHES, Ieda Del'Arco. **Sensoriamento Remoto em Agricultura**. São Paulo: Oficina de Textos, 2017. Disponível em: https://ebooks.ofitexto.com.br/product/sensoriamento-remoto-em-agricultura%0Ahttps://ebooks.ofitexto.com.br/epubreader/sensoriamento-remoto-em-agricultura.

GALVÃO, Lênio Soares; FORMAGGIO, Antônio Roberto; TISOT, Daniela Arnold. DISCRIMINAÇÃO DE VARIEDADES DE CANA-DE-AÇÚCAR COM DADOS HIPERESPECTRAIS DO SENSOR HYPERION/EO-1. **Revista Brasileira de Cartografia**, *[S. l.]*, v. 57, n. 1, p. 7–14, 2005. Disponível em: http://www.seer.ufu.br/index.php/revistabrasileiracartografia/article/view/44957.

GAMON, J. A.; SERRANO, L.; SURFUS, J. S. The photochemical reflectance index: an optical indicator of photosynthetic radiation use efficiency across species, functional types, and nutrient levels. **Oecologia**, *[S. l.]*, v. 112, n. 4, p. 492–501, 1997. DOI: 10.1007/s004420050337.

GAUI, Tatiana Dias; COSTA, Flávia Regina Capellotto; COELHO DE SOUZA, Fernanda; AMARAL, Márcio Rogério Mota; DE CARVALHO, Daniel Costa; REIS, Francisco Quintiliano; HIGUCHI, Niro. Long-term effect of selective logging on floristic composition: A 25 year experiment in the Brazilian Amazon. **Forest Ecology and Management**, *[S. l.]*, v. 440, p. 258–266, 2019. DOI: https://doi.org/10.1016/j.foreco.2019.02.033. Disponível em: https://www.sciencedirect.com/science/article/pii/S0378112718323272.

HOPE, Mat. The Brazilian development agenda driving Amazon devastation. **The Lancet Planetary Health**, *[S. l.]*, v. 3, n. 10, p. e409--e411, 2019. DOI: 10.1016/s2542-5196(19)30195-0. Disponível em: https://doi.org/10.1016/s2542-5196(19)30195-0.

INOUE, Y.; PEÑUELAS, J.; MIYATA, A.; MANO, M. Normalized difference spectral indices for estimating photosynthetic efficiency and capacity at a canopy scale derived from hyperspectral and CO2 flux measurements in rice. **Remote Sensing of Environment**, *[S. l.]*, v. 112, n. 1, p. 156–172, 2008. DOI: https://doi.org/10.1016/j.rse.2007.04.011. Disponível em: https://www.sciencedirect.com/science/article/pii/S003442570700185X.

JAMES B. CAMPBELL, Randolph H. Wynne. **Introduction to Remote Sensing**. 5. ed. New York: Guilford Press, 2011.

KHDERY, Ghada; YONES, Mona. Innovative spectral library for identification common wild plants using hyperspectral technology in Northwestern Coast, Egypt. **Egyptian Journal of Remote Sensing and Space Science**, *[S. l.]*, n. xxxx, 2020. DOI: 10.1016/j.ejrs.2020.08.002. Disponível em: https://doi.org/10.1016/j.ejrs.2020.08.002.

LILLESAND, Thomas M.; KIEFER, Ralph W. **Remote sensing and image interpretation**. 3. ed. New York: John Wiley e Sons Inc., 1994.

LU, Yao; WANG, Wei; NI, Xinzhi; ZHUANG, Hong. Non-destructive discrimination of Illicium verum from poisonous adulterant using Vis/NIR hyperspectral imaging combined with chemometrics. **Infrared Physics and Technology**, *[S. l.]*, v. 111, n. September, p. 103509, 2020. DOI: 10.1016/j.infrared.2020.103509. Disponível em: https://doi.org/10.1016/j.infrared.2020.103509.

MENESES, Paulo Roberto; ALMEIDA, Tati De; ROSA, Antonio Nuno de Castro Santa; SANO, Edson Eyji; SOUZA, Edilson Bias De; BAPTISTA, Gustavo Macedo de Mello; BRITES, Ricardo Seixas. **Introdução Ao Processamento de Imagens de Sensoriamento Remoto**. 1. ed. Brasília.

MURO, Javier; DONINCK, Jasper Van; TUOMISTO, Hanna; HIGGINS, Mark A.; MOULATLET, Gabriel M.; RUOKOLAINEN, Kalle. Floristic composition and across-track reflectance gradient in Landsat images over Amazonian forests. **ISPRS Journal of Photogrammetry and Remote Sensing**, *[S. l.]*, v. 119, p. 361–372, 2016. DOI: 10.1016/j.isprsjprs.2016.06.016. Disponível em: http://dx.doi.org/10.1016/j.isprsjprs.2016.06.016.

NIDAMANURI, Rama Rao. Hyperspectral discrimination of tea plant varieties using machine learning, and spectral matching methods. **Remote Sensing Applications: Society and Environment**, *[S. l.]*, v. 19, p. 100350, 2020. DOI: https://doi.org/10.1016/j.rsase.2020.100350. Disponível em: https://www.sciencedirect.com/science/article/pii/S235293852030121X.

OUÉDRAOGO, D. Y.; BEINA, D.; PICARD, N.; MORTIER, F.; BAYA, F.; GOURLET-FLEURY, S. Thinning after selective logging facilitates floristic composition recovery in a tropical rain forest of Central Africa. **Forest Ecology and Management**, *[S. l.]*, v. 262, n. 12, p. 2176–2186, 2011. DOI: 10.1016/j.foreco.2011.08.009. Disponível em: https://doi.org/10.1016/j.foreco.2011.08.009.

PEREIRA, Maria do Socorro; ALVES, Rômulo Romeu da Nóbrega. Composição Florística de um remanescente de Mata Atlântica na Área de Proteção Ambiental Barra

do Rio Mamanguape, Paraíba, Brasil. **Revista de Biologia e Ciências da Terra**, *[S. l.]*, v. 7, n. 1, p. 1–10, 2007. Disponível em: https://www.redalyc.org/pdf/500/50007101.pdf.

PONZONI, Flávio Jorge; SHIMABUKURO, Yosio Edemir. **Sensoriamento remoto no estudo da vegetação**. São José dos Campos: Parêntese Editora, 2009.

RAHMAN, Abdullah F.; GAMON, John A.; FUENTES, David A.; ROBERTS, Dar A.; PRENTISS, Dylan. Modeling spatially distributed ecosystem flux of boreal forest using hyperspectral indices from AVIRIS imagery. **Journal of Geophysical Research: Atmospheres**, *[S. l.]*, v. 106, n. D24, p. 33579–33591, 2001. DOI: 10.1029/2001jd900157.

ROUSE J. W., Jr.; HAAS, R. H.; SCHELL, J. A.; DEERING, D. W. Monitoring Vegetation Systems in the Great Plains with ERTS. In: PROCEEDING OF ERTS-1 SYMPOSIUM 1974, **Anais** [...]. [s.l: s.n.] p. 309.

SILVA, Caetano Affonso Couto Podlasinski; SILVA-JUNIOR, Carlos Antonio Da; SHIRATSUCHI, Luciano Shozo; LIMA, Mendelson; ROSSI, Fernando Saragosa; SANTOS, Reginaldo Carvalho. Discriminação hiperespectral de mudas de Eucaliptus urophylla x Eucaliptus camaldulensis (VM-01) em condição de deficiência e toxicidade de boro. *In*: ANAIS DO XIX SIMPÓSIO BRASILEIRO DE SENSORIAMENTO REMOTO 2019, Santos. **Anais** [...]. Santos: INPE, 2019. DOI: 10.13140/RG.2.2.28177.07527. Disponível em: http://dx.doi.org/10.13140/RG.2.2.28177.07527.

SILVA JUNIOR, Carlos Antonio Da et al. Soybean varieties discrimination using non-imaging hyperspectral sensor. **Infrared Physics &Technology**, *[S. l.]*, v. 89, p. 338–350, 2018. DOI: 10.1016/j.infrared.2018.01.027. Disponível em: https://doi.org/10.1016/j.infrared.2018.01.027.

SILVA JUNIOR, Carlos Antonio Da; COSTA, Gerlane de Medeiros; ROSSI, Fernando Saragosa; VALE, Jôine Cariele Evangelista Do; LIMA, Rogério Brito De; LIMA, Mendelson; OLIVEIRA-JUNIOR, José Francisco De; TEODORO, Paulo Eduardo; SANTOS, Reginaldo Carvalho. Remote sensing for updating the boundaries between the brazilian Cerrado-Amazonia biomes. **Environmental Science and Policy**, *[S. l.]*, v. 101, n. April, p. 383–392, 2019. a. DOI: 10.1016/j.envsci.2019.04.006. Disponível em: https://doi.org/10.1016/j.envsci.2019.04.006.

SILVA JUNIOR, Carlos Antonio Da; DE MEDEIROS COSTA, Gerlane; ROSSI, Fernando Saragosa; DO VALE, Jôine Cariele Evangelista; DE LIMA, Rogério Brito; LIMA, Mendelson; DE OLIVEIRA-JUNIOR, José Francisco; TEODORO, Paulo

Eduardo; SANTOS, Reginaldo Carvalho. Remote sensing for updating the boundaries between the brazilian Cerrado-Amazonia biomes. **Environmental Science & Policy**, *[S. l.]*, v. 101, p. 383–392, 2019. b. DOI: 10.1016/j.envsci.2019.04.006.

SILVERSTEIN, Robert; WEBSTER, Francis X.; KIEMLE, David J.; BRYCE, David L. **Spectrometric identification of organic compounds**. Hoboken, NJ: Wiley, 2015.

SOUZA, Agostinho. **Florestas nativas: estrutura, dinâmica e manejo**. Viçosa, MG, Brasil: Editora UFV Universidade Federal de Viçosa, 2013.

SOUZA, Ana Paula Damasceno; TEODORO, Paulo Eduardo; TEODORO, Larissa Pereira Ribeiro; TAVEIRA, Aline Cordeiro; DE OLIVEIRA-JÚNIOR, José Francisco; DELLA-SILVA, João Lucas; BAIO, Fabio Henrique Rojo; LIMA, Mendelson; DA SILVA JUNIOR, Carlos Antonio. Application of remote sensing in environmental impact assessment: a case study of dam rupture in Brumadinho, Minas Gerais, Brazil. **Environmental Monitoring and Assessment**, *[S. l.]*, v. 193, n. 9, p. 606, 2021. DOI: 10.1007/s10661-021-09417-z. Disponível em: https://doi.org/10.1007/s10661-021-09417-z.

TADDEO, Sophie; DRONOVA, Iryna; HARRIS, Kendall. ISPRS Journal of Photogrammetry and Remote Sensing Greenness, texture, and spatial relationships predict floristic diversity across wetlands of the conterminous United States. **ISPRS Journal of Photogrammetry and Remote Sensing**, *[S. l.]*, v. 175, n. September 2020, p. 236–246, 2021. DOI: 10.1016/j.isprsjprs.2021.03.012. Disponível em: https://doi.org/10.1016/j.isprsjprs.2021.03.012.

VAIPHASA, Chaichoke; SKIDMORE, Andrew K.; DE BOER, Willem F.; VAIPHASA, Tanasak. A hyperspectral band selector for plant species discrimination. **ISPRS Journal of Photogrammetry and Remote Sensing**, *[S. l.]*, v. 62, n. 3, p. 225–235, 2007. DOI: 10.1016/j.isprsjprs.2007.05.006.

VANE, G.; GOETZ, A. F. H. Terrestrial imaging spectrometry: Current status, future trends. **Remote Sensing of Environment**, United States, v. 43, n. 2–3, p. 117–126, 1993. Disponível em: http://inis.iaea.org/search/search.aspx?orig_q=RN:24072258.

VENTER, Sarah M.; WITKOWSKI, Ed T. F. Phenology, flowering and fruit-set patterns of baobabs, Adansonia digitata, in southern Africa. **Forest Ecology and Management**, *[S. l.]*, v. 453, p. 117593, 2019. DOI: 10.1016/j.foreco.2019.117593. Disponível em: https://doi.org/10.1016/j.foreco.2019.117593.

WEST, Jonathan S.; BRAVO, Cedric; OBERTI, Roberto; MOSHOU, Dimitrios;

RAMON, Herman; MCCARTNEY, H. Alastair. Detection of Fungal Diseases Optically and Pathogen Inoculum by Air Sampling. *In*: **Precision Crop Protection - the Challenge and Use of Heterogeneity**. [s.l.]: Springer Netherlands, 2010. p. 135–149. DOI: 10.1007/978-90-481-9277-9_9. Disponível em: https://doi.org/10.1007/978-90-481-9277-9_9.

YU, Keqiang; FANG, Shiyan; ZHAO, Yanru. Heavy metal Hg stress detection in tobacco plant using hyperspectral sensing and data-driven machine learning methods. **Spectrochimica Acta - Part A: Molecular and Biomolecular Spectroscopy**, *[S. l.]*, v. 245, p. 118917, 2021. DOI: 10.1016/j.saa.2020.118917. Disponível em: https://doi.org/10.1016/j.saa.2020.118917.

CHAPTER I.
IS IT POSSIBLE TO IDENTIFY AMAZONIAN FOREST SPECIES USING SPECTROSCOPY APPROACH?

The present manuscript will follow the standards adopted by the journal *Environmental Monitoring and Assessment*, to which the present work will be submitted.

CHAPTER I.

IS IT POSSIBLE TO IDENTIFY AMAZONIAN FOREST SPECIES USING SPECTROSCOPY APPROACH?

João Lucas Della Silva [1], Carlos Antonio da Silva Junior [2,*], Mendelson Lima [3], Ricardo da Silva Ribeiro [4], Luciano Shozo Shiratsuchi [5], Fernando Saragosa Rossi [6], Larissa Pereira Ribeiro Teodoro [7], and Paulo Eduardo Teodoro [7]

1 Federal University of Mato Grosso (UFMT), Post-Graduate Program in Environmental Sciences (PPGCAM), Sinop, Mato Grosso, Brazil.;
2 State University of Mato Grosso (UNEMAT), Sinop, Mato Grosso, Brazil;
3 State University of Mato Grosso (UNEMAT), Alta Floresta, Mato Grosso, Brazil;
4 National Institute of the Atlantic Forest (INMA), Santa Teresa, Espírito Santo, Brazil;
5 Louisiana State University (LSU), AgCenter, School of Plant, Environmental, and Soil Sciences, Baton Rouge, Louisiana, United States;
6 State University of São Paulo (UNESP), Jaboticabal, São Paulo, Brazil;
7 Federal University of Mato Grosso do Sul (UFMS), Chapadão do Sul, Mato Grosso do Sul, Brazil.

* Correspondence: carlosjr@unemat.br; ORCID: 0000-0002-7102-2077

ABSTRACT

Sampling trees in natural environment can be used in studies ranging from floristic composition and phytogeography to management and growth modelling, and accurate inventories are based on highly labor-intensive methods. Relying on hyperspectral approach, this study aimed to differentiate spectral libraries of four Amazon tree species. We first prepared the spectroradiometer data on representative bands on foliar biochemistry, followed by reflectance inflection difference and finally, we applied spectral vegetation models. Next, the discriminant analysis was reasoned on multivariate approach, were successfully discriminated the spectral curves related to each of evaluated tree species. By visual analysis, some regions of the electromagnetic spectrum with higher differentiation in reflectance responses can be seen, in portions of the visible spectrum (0.5 - 0.65 μm), near-infrared (0.913 – 1.25 μm) and short-wave infrared 2 (2.1 – 2.5 μm). There was a higher contribution in distinguishing between species based on specific RID (Reflectance Inflection Difference) heights, such as seen on specific representative bands. Principal component (PC) analysis applied to the vegetation spectral models brought satisfactory results, with PC1 highly related to the variability of the vegetation indices results (99.37%). Adopting this approach in hyperspectral data at the leaf level and well-defined classes results in good responses. We emphasize the importance of using combined vegetation indices, with greater contributions by

indices developed for quantization or absorption of electromagnetic radiation by chlorophyll, which are based in the visible region.

Keywords: Amazonian trees; leaf-based data; hyperspectral libraries; multivariate analysis; vegetation indices; forest management; tree species classification.

1.INTRODUCTION

The accurate floristic classification of an area is based on the sampling or census of individuals, which is a highly labor-intensive task (Kersten & Galvão, 2011; Thomas et al., 2012). Inventory methods with well-established criteria such as the plot system (Ellenberg and Mueller-Dombois 1974) and walking (Filgueiras et al. 1994) are observed, in addition to subjective criteria such as the choice of homogeneous stretches (Rodal et al. 2013), combination of methods or automated methods (Feeley and Silman 2009; Ter Steege et al. 2013).

Sampling trees in a natural environment can be used in studies ranging from floristic composition and phytogeography to vegetation management and growth modeling, and efficiently depends on knowledge of sampling procedures and statistical principles, which are the basis of plant sampling methods (Jeanine Maria Felfili et al. 2011). The floristic survey is one of the main types of diagnosis and classification of the plant communities in an environment, and from the survey, several aspects of the natural vegetation dynamics in forest environments can be understood (Watt 1947). Furthermore, Amazon biome lacks investigations regarding the identification (Cardoso et al. 2017) and richness of species (Ter Steege et al. 2016) and diversity patterns (Ter Steege et al. 2019), even more so when considering the biome with the greatest biodiversity in the world (Feeley and Silman 2011). Listing and monitoring the flora is essential for political and legal efforts to conserve species, especially when they are under threat of extinction (Brandes et al. 2020).

Among the technologies to perform such a survey, spectroscopy is applied in studies of vegetation classification, in terms of species (Clark et al. 2005; Mudereri et al. 2020; Vaiphasa et al. 2007), varieties of the same species (Nidamanuri 2020; Silva et al. 2019; Silva Junior et al. 2018), water content (Brito and Farias 2013; Clevers et al. 2008, 2010), plant growth rate (Luís Guilherme Teixeira Crusiol et al.

2021) e changes in chemical composition, such as boron deficiency (Dong et al. 2018) or due to the arrangement of the individual in a planting stand (Brandelero et al. 2012).

In this regard, the floristic survey can be based on in-situ spectroscopy data, which for remote sensing science is the reference hyperspectral database for remote observations (Crusiol et al., 2019), and thus provide the database for agile and accurate observations (Baldeck et al. 2015; Lang et al. 2015; Vaglio Laurin et al. 2014).

Spectroradiometer spectroscopy provides a significant volume of data, with a high spectral resolution basis (Kishore et al. 2020; Malvern Panalytical 2019). Transformation of an enormity of data is commonly accomplished through spectral models of vegetation, where data is maximized to observe relative abundance, vegetation activity, or any biophysical parameters of interest (M. S. Flores et al. 2020; J. Jensen 2007), or even highlight vegetation from other targets (Caturegli et al. 2014; Peng et al. 2021). From the perspective of differentiating plant species using spectral data, plant differentiation studies like this one can take Principal Component (PC) analysis (Gomes et al. 2020) and cluster analysis (CA) (Furlanetto et al. 2020; Silva Junior et al. 2018) as the statistical basis.

In view of the above and of the difficulties in field identification, the objective of this study was to verify the ability to distinguish tree species in the Southern Brazilian Amazon using hyperspectral remote sensing in a native flora area, observing four species of economic interest for timber extraction [*Schizolobium parahyba* (Vell.) Blake (Romão and Mansano 2020) and *Cedrela fissilis* Vell. (Flores, 2020)] and forest products for other purposes [*Berthollethia excelsa* (Ribeiro et al. 2020) and *Euterpe oleracea* Mart. (Vianna 2020)], as well as establishing a spectral library standard for each species.

2. Materials and Methods

2.1 Characterization and geographical location

The study area comprises the municipality of Alta Floresta (Latitude 09º52'32 "S and Longitude 56º05'10 "W), Mato Grosso, located in the Southern Amazon (Figure 1). Alta Floresta has an altitude of approximately 283 meters and a tropical climate. Two well-defined seasons occur, a wet and a dry period. According to the Köppen-Geiger classification, the region climate is Aw type, with average

temperature ranging around 26.4°C, and average annual rainfall reaching 2,281 mm (Alvares et al. 2013).

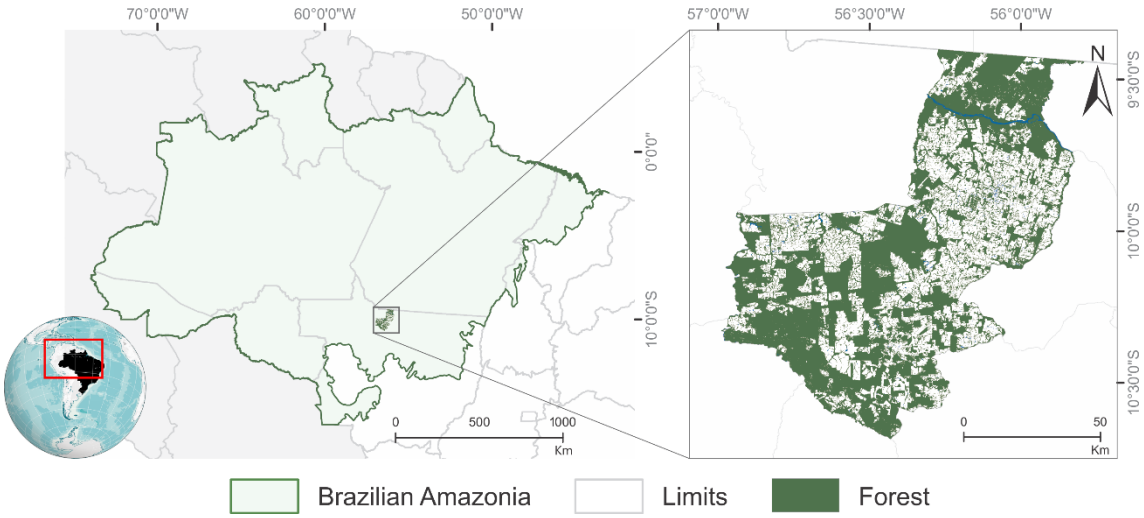

Figure 1. Location map of the Brazilian Amazon (IBGE, 2019), followed by the map of forest areas in the municipality of Alta Floresta, in the northern region of the state of Mato Grosso, Brazil.

2. 2 Native Species Analyzed

The biodiversity of the Amazonian flora is important for the culture and economy of human populations living in the biome, especially for extractive activities (Homma 2011a), where bioprospecting activities enhance the global market expansion of non-timber forest products (Balzon et al. 2004). Besides the products, selective timber extraction is the most primal practice given the demand for human consumption (Homma 2011b). From these considerations, the definition of the tree species included in this analysis are, in part, species for logging, and in another part, non-timber forest products (NTFP) tree species.

Given the above, the following plant species were considered:

- *Bertholletia excelsa* Bonpl. - Lecythidaceae (Brazil nut tree, "Castanheira-do-Brasil"), species that has great cultural and economic value when it comes to both timber value and NTFPs, considering the consumption of the seed and the use of wood, when legalized. The species is threatened with extinction and is in the Vulnerable (VU) category in the Brazilian territory. (Martinelli and Moraes 2013). The trees grow up to 60 meters in height and are canopy trees. It has

simple oblong leaves, with lengths between 25 and 35 centimeters and widths between 8 and 12 centimeters (Ribeiro et al. 2020; Souza et al. 2008);

- *Euterpe oleracea* Mart. – Arecaceae ("Açaizeiro"), has as products the fruit and the palm heart, which are consumed globally (species with the highest value in NTFP production). Cepitose palm with an erect stem reaching heights from 3 to 20 meters. It has 40 to 80 pairs of Folioles hanging from a compound pinnate leaf, with length between 20 and 50 centimeters and width ranging from 2 to 3 centimeters (Henderson and Galeano 1996);
- *Schizolobium parahyba* (Vell.) Blake – Fabaceae (Cuiabano pine), species with great value in timber extraction, with a height of up to 40 meters. It has bipinnate leaves that are 80 to 100 centimeters long, with 6 to 29 pairs of pinnae and 9 to 30 pairs of Folioles (Richter et al. 1974);
- *Cedrela fissilis* Vell. – Meliaceae (cedar tree, "Cedro-Rosa"), has great economic value due to its lumber with great added value and social value. It is an endangered species, in the Vulnerable (VU) category (Martinelli and Moraes 2013). Tree 8-30 meters high. Pinate compound leaves with 50 to 120 centimeters long and 10 to 17 pairs of Folioles (Flores, 2020). Folioles with length between 7 and 14 centimeters and width between 3 and 4 centimeters (Grings and Brack 2011).

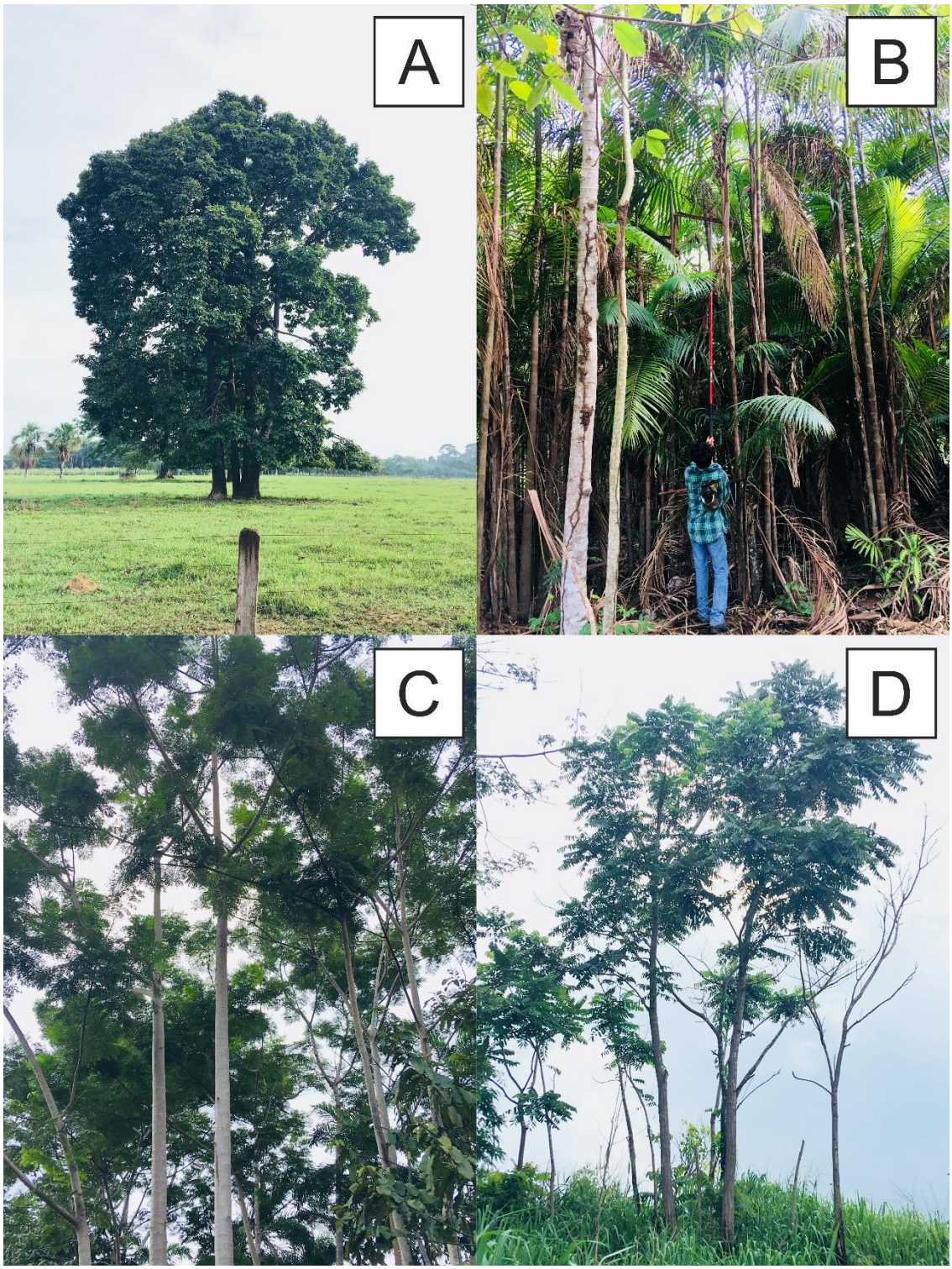

Figure 2. Amazonian trees studied, where: A - *Bertholletia excelsa*; B – *Euterpe oleracea*; C – *Schizolobium parahyba*; D – *Cedrela fissilis*.

The samples collected were healthy leaves from the top of mature trees, which were removed with a tree pruner (procedure shown in Figure 2B). The leaves at the top of the tree were chosen since these data most closely resemble those

generated remotely (orbital or airbone), and seeking data closer to natural occurrence, these leaves were removed from random mature individuals in a forest in the study area, and immediately submitted to the spectroradiometer.

2.3 Hyperspectral Curve Acquisition

Radiometric readings were performed using the FieldSpec® 4 Hi-Res, which is a high spectral resolution spectroradiometer designed for faster and more accurate spectral data measurements for a wide range of remote sensing applications. The spectroradiometer's 3 nm spectral resolution VIS and NIR (Visible and Near Infrared) and 8 nm SWIR (Shortwave Infrared) provide superior spectral performance across the full range solar irradiance spectrum (0.35-2.5 μm). Enhanced spectral resolution in the SWIR range (1.0-2.5 μm) is particularly useful for detecting and identifying compounds with narrow spectral characteristics at longer wavelengths (Malvern Panalytical 2019).

Furthermore, the 8 nm resolution meets or exceeds the spectral resolution of most hyperspectral sensors, making the FieldSpec® 4 Hi-Res spectroradiometer an excellent choice for sensor validation and calibration, as well as ground data exchange and spectral library construction.

For the spectral reading of each leaf, the ASD *Plant Probe* was used. This equipment is used for leaf measurements, and its main characteristic is the non-destructive method, with no interference from the luminosity of the reading site; it is 25.4 cm long, weighs 0.7 kg, and has a 6.5 W lamp. ASD *Plant Probe* is designed for contact spectral measurements of solid raw materials. With this accessory, it is possible to minimize errors associated with stray light by also allowing the analysis of samples through transparent plastic bags.

Spectral readings were repeated three times (one on each leaf) for different individuals for each tree species, namely Brazil nut tree (*Berthollethia excelsa* Bonpl.), "Açaí" tree (*Euterpe oleracea* Mart.), Cuiabano pine *(Schizolobium parahyba* (Vell.) Blake), and cedar tree (*Cedrela fissilis* Vell.). In this study, spectral data were based on the adaxial face of leaf samples, more closely related to airborne or orbital imagery data. These data were obtained based on the average of the three readings for each sample (Chicati 2011; Fiorio et al. 2010; Nanni and

Dematte 2000). The samples for this procedure were characterized as mature leaves (Chavana-Bryant et al. 2019).

The equipment used depends on a reference standard, where barium sulfate was used ($BaSO_4$), a white plate of the device itself which reflects 100% of the light beam. The spectral data from this plate is stored by the system for later determination of the reflectance factor of the samples, where they are weighted by the readings obtained from each sample.

2.4 Spectral data preparing for analyses

Here, were applied three dimensionality reduction methods, in order to generating the datasheet used in the statistical analyses. The first method is selecting the bands and inflection heights (Nanni et al. 2004; Silva Junior et al. 2020) and its reflectances level. The selected band is based on the average wavelength range at different points in the analyzed spectrum (0.35 to 2.5 μm). This selection is based on visual observations of the average spectral curves and the known vegetation spectral curves described in Figure 3.

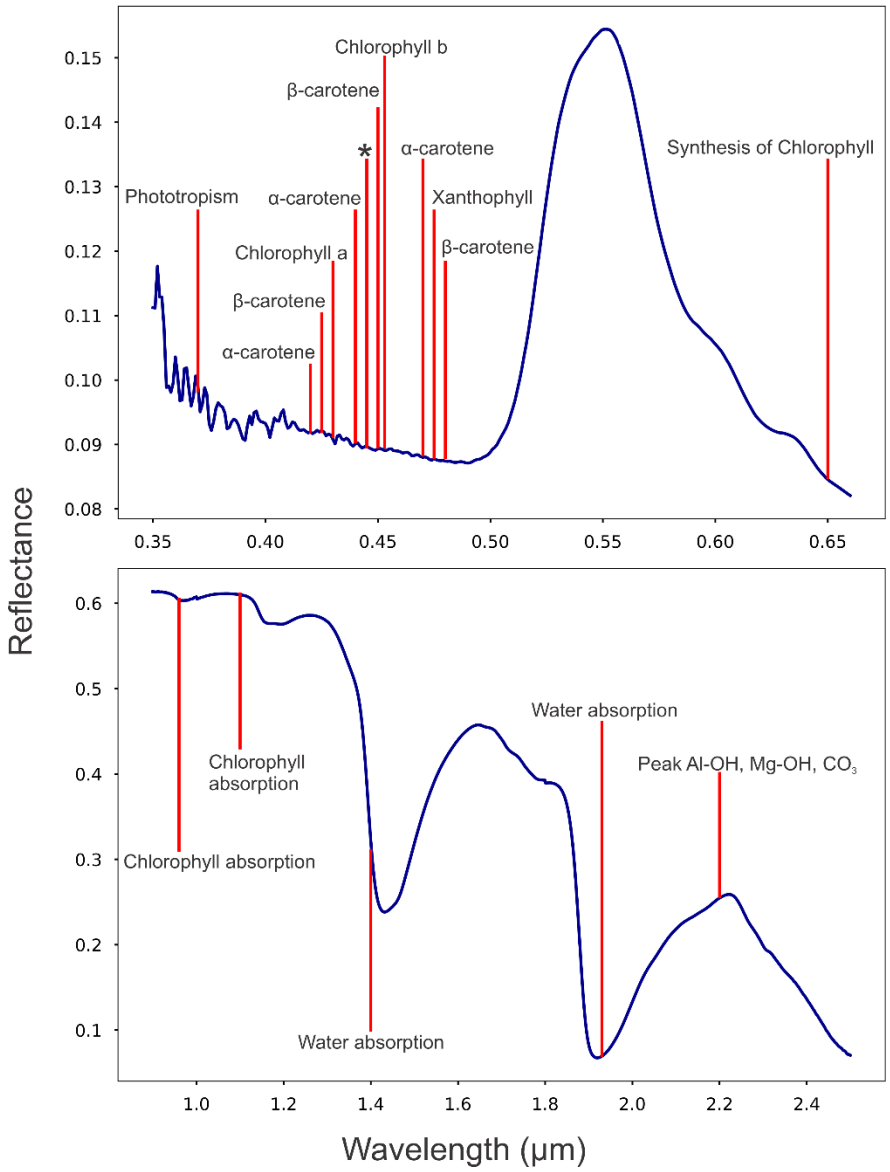

Figure 3 – Vegetative characteristics and their centered spectral responses. *Xanthophyll and Chlorophyll Synthesis.

Next, the spectral curve intervals between inflections, bulged and concave portions, present in the mean curves of all native Amazonian species evaluated, were classified. In addition to the average interval, the wavelength characterized by a strong inflection was used.

The spectral behavior related to its reflectance shows the averages of representative wavelength intervals and sharp inflection points representing elements known as phototropism, a and b carotene, and water (Marshak and Knyazikhin 2017). The division into 28 VIS and infrared bands of the electromagnetic spectrum is detailed in Table 1 (Silva Junior et al. 2018).

Table 1. Wavelength ranges that will be used to establish 28 spectral bands for statistical treatment.

Bands (n°)	Spectral Range (µm)	Average Wavelength (µm)
1	0.35-0.369	0.359
2	0.370	0.37
3	0.371-0.419	0.395
4	0.420	0.42
5	0.421-0.424	0.422
6	0.425	0.425
7	0.426-0.444	0.435
8	0.445-0.475	0.46
9	0.480	0.48
10	0.481-0.500	0.49
11	0.501-0.530	0.515
12	0.531-0.539	0.535
13	0.540	0.54
14	0.541-0.649	0.595
15	0.650	0.65
16	0.661-0.670	0.665
17	0.675	0.675
18	0.676-0.684	0.680
19	0.685-0.689	0.687
20	0.690-0.700	0.695
21	0.701-0.709	0.705
22	0.710	0.71
23	0.711-0.730	0.72
24	0.960	0.96
25	1.100	1.1
26	1.400	1.4
27	1.930	1.93

28	2.200	2.2

The second way of selecting spectral curves obtained by spectroradiometric analyses is using the difference between the reflectance factor value centered on the smallest inflection point (absorption bands) and the reflectance factor value on the next largest point, called the crest. These ranges are called reflectance inflection difference (RID) and were determined as shown in Figure 4. A visual analysis of the spectral curves for a given species indicates the presence of 22 heights (or spectral bands) throughout the analyzed spectrum, described in Table 2 (Silva Junior et al. 2020). It is important to note that the 22 heights of this selection method are not related to the aforesaid 28 representative wavelengths.

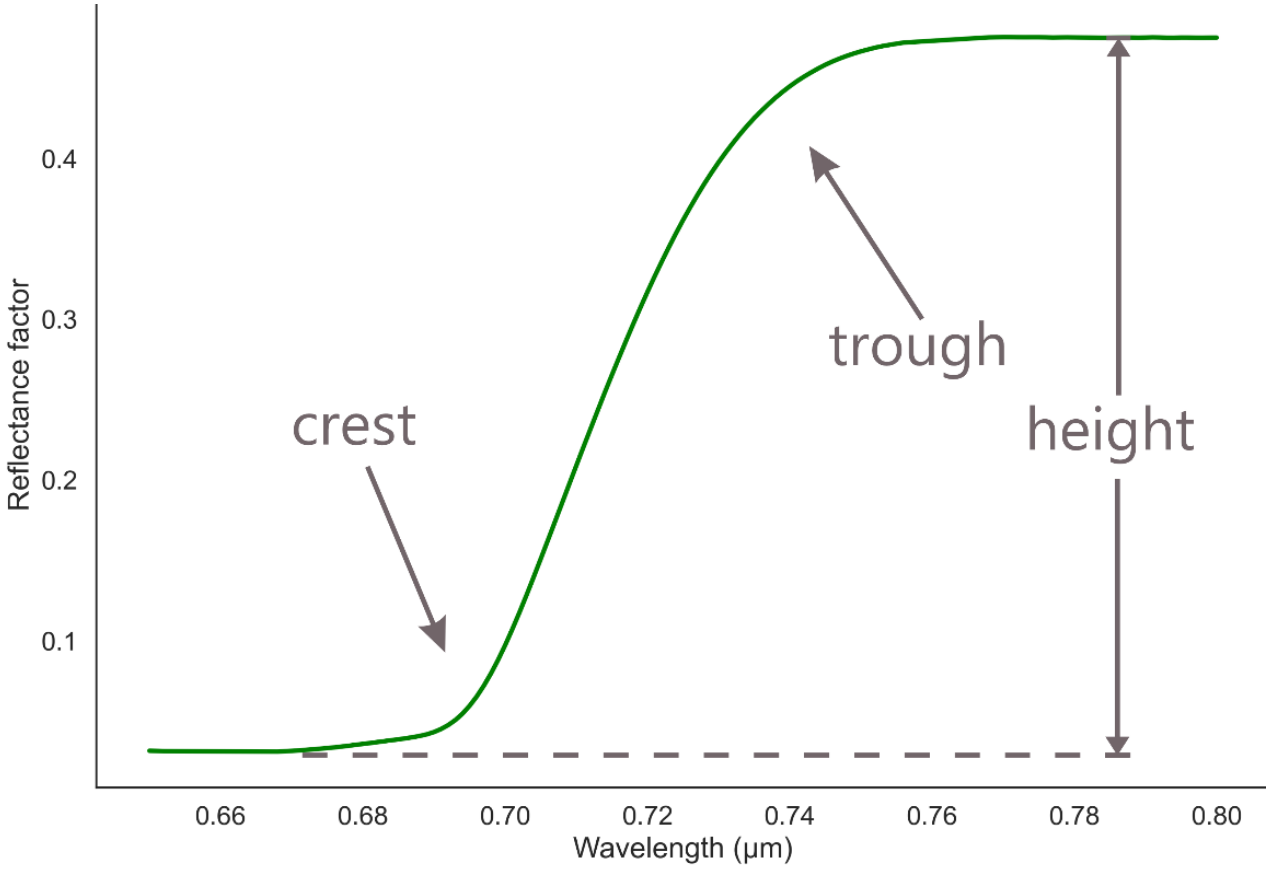

Figure 4. Methodology for determining interband heights (RID) for spectral curves.

Table 2. Reflectance difference inflections (RID) selected for the statistical analysis.

Height (h)	Spectral Range (μm)
1	0.350-0.371
2	0.389-0.405
3	0.479-0.530
4	0.531-0.537
5	0.540-0.573
6	0.586-0.611
7	0.621-0.652
8	0.668-0.756
9	0.768-0.892
10	0.913-0.947
11	0.948-0.983
12	0.984-0.992
13	0.993-1.034
14	1.102-1.172
15	1.186-1.257
16	1.270-1.427
17	1.428-1.634
18	1.652-1.792
19	1.811-1.910
20	1.948-2.115
21	2.124-2.208
22	2.215-2.450

The data spreadsheet was prepared based on the 28 bands obtained by averaging the optical spectrum intervals, as well as the specific absorptions, with 22 reflectance factor height (RID) values for each native Amazonian Forest species variety.

2.5 Calculation of Spectral Vegetation Models

We used the values relative to the average spectral curves obtained through the spectroradiometer, which in turn are based on the average values of the blue, green, red, and near-infrared bands. Among the vegetation indices applied, the EVI (*Enhanced Vegetation Index*) (Huete et al. 1997) can be obtained by Equation 1.

$$EVI = g.\frac{\rho_{NIR}-\rho_{RED}}{\rho_{NIR}+(c_1.\rho_{RED})-(c_2.\rho_{BLUE})+l} \quad (1)$$

Wherein:

ρ_{NIR} , ρ_{RED} and ρ_{BLUE}: reflectance in the near-infrared, red and blue spectral ranges, respectively;

g: gain factor (2.5);

c_1 and c_2: are the correction coefficients for atmospheric effects for red (6) and blue (7.5), respectively;

l: correction factor for soil interference.

The EVI is an index that was developed to mitigate the effects of the soil (adjusted by Soil Adjusted Vegetation Index - SAVI) and the atmosphere (adjusted by ARVI) in vegetation mapping. In addition to EVI, NDVI (Equation 2) was used in this analysis.

$$NDVI = \frac{\rho_{NIR} - \rho_{RED}}{\rho_{NIR} + \rho_{RED}} \quad (2)$$

Wherein:

ρ_{NIR} and ρ_{RED}: reflectances in the near-infrared and red spectral range, respectively.

The NDVI is the most widespread and widely used spectral model in remote sensing (Cohen and Justice 1999). Among the vegetation indices, the GNDVI (*Green Normalized Difference Vegetation Index*) is given by Equation 3 (Gitelson et al. 1996).

$$GNDVI = \frac{(\rho NIR-\rho GRE)}{(\rho NIR+\rho GRE)} \quad (3)$$

Wherein:

ρNIR: near-infrared band;

$\rho Green$: green band.

Although the EVI and NDVI indices have been widely used, they present some limitations, such as interference from soil color and moisture effects. Thus, an index that could improve NDVI considering the canopy substrate. To this end, SAVI (*Soil Adjusted Vegetation Index*) was developed from a constant "L" as an adjustment factor for this canopy substrate. In this way, the SAVI is obtained using Equation 4.

$$SAVI = (1 + L)\frac{(\rho NIR - \rho RED)}{(\rho NIR + \rho RED + L)} \quad (4)$$

Wherein:
L= 0.5;
ρNIR: near-infrared band;
ρRED: red band.

The constant "L" shows values from 0 to 1, varying according to the biomass itself. The optimal values for "L" are: L = 1 (for low vegetation densities); L = 0.5 (for medium vegetation densities); and L = 0.25 (for high vegetation densities) (Huete et al. 1997). Overall, the factor L = 0.5 is commonly used, since it encompasses a higher variation of vegetation conditions. Still, the SAVI is limited due to different biomes and agricultural situations since the constant values are generalized, not considering the specificities of the environments analyzed, but only the vegetation density (Ponzoni and Shimabukuro 2009).

The Transformed Vegetation Index (Broge and Leblanc 2001), defined by the acronym TVI, describes the radiative energy absorbed by pigments as a function of the relative difference between reflectance in the red and near-infrared together with the magnitude of reflectance in the green region, where light absorption by chlorophyll a and b is relatively insignificant (J. R. Jensen 2009). Equation 5 was used to obtain the TVI.

$$TVI: \sqrt{NDVI + 0.5} \quad (5)$$

Wherein:

NDVI: Normalized Difference Vegetation Index.

The *Optimized Soil Adjusted Vegetation Index* (OSAVI) is a variation of SAVI, suitable for monitoring agricultural crops (Rondeaux et al. 1996). From evaluating several coefficients in different indices, the authors mentioned above obtained the best fit with a value of 0.16. The advantage of OSAVI over the other indices dependent on the soil line is that without knowing the soil line, it can be determined, i.e., it does not require a priori knowledge of the soil type (Steven 1998). The OSAVI is given by Equation 6.

$$OSAVI = (1 + Y)\frac{(\rho NIR - \rho RED)}{(\rho NIR + \rho RED + Y)} \quad (6)$$

Wherein:
$Y = 0.16$
ρNIR: near infrared band;
ρRED: red band.

Characterizing the leaf nitrogen (N) content based on the chlorophyll A content, the concentration of this substance sensitizes the reflectance at certain wavelengths, where higher concentrations sensitize the reflectance at 548 nanometers and lower concentrations sensitize the reflectance at 672 nanometers (Jacquemoud and Baret 1990). This proposes a correlation between chlorophyll-a and nitrogen content (Filella et al. 1995), which can be the basis for choosing a vegetation index to distinguish between species.

NPCI – *Normalized Pigment Chlorophyll Index* (Peñuelas et al. 1994) is based on these nitrogen-sensitive wavelengths, which proposes a quantification of the effects of different concentrations of this substance in the plant canopy (Equation 7).

$$NPCI = \frac{\rho 680nm - \rho 430nm}{\rho 680nm + \rho 430nm} \quad (7)$$

Wherein:

$\rho 680nm$: reflectance at 680 nanometers;
$\rho 430nm$: reflectance at 430 nanometers.

In terms of evaluating the absorbed photosynthetically active fraction, the CARI2 index was designed to minimize the effect of non-photosynthesizing targets on the vegetation (Kim 1994). It is characterized as an index based on high spectral resolution, which is satisfied in applications with the FieldSpec® 4.

$$CARI2 = \left(\frac{a \times \rho 670nm + \rho 670nm + b}{(a^2+1)^{0,5}}\right) \times \left(\frac{\rho 700nm}{\rho 670nm}\right) \quad (8)$$

Wherein:

$a = \rho 700nm - \rho 550nm$

$b = \rho 550nm - a \times \rho 550nm$

$\rho 700nm$: reflectance at 700 nanometers;

$\rho 670nm$: reflectance at 670 nanometers;

$\rho 550nm$: reflectance at 550 nanometers;

In the identification and classification of different plant species that occur in a natural environment, the behavior of electromagnetic radiation in the red edge is responsible for a great contribution (Chatziantoniou et al. 2017; Liu et al. 2021). Red edge position and size are used as indicators of chlorophyll content, biomass, and water status of plant targets (Filella and Peñuelas 1994). Among the vegetation indices, the LCI (*Leaf Chlorophyll Index*) is based on the red, mid-infrared, and red edge bands, representing the shape of the spectral curve near this range (Datt 1999).

From a plant canopy-based perspective, the LCI is a chlorophyll-sensitive vegetation index over a significant range of chlorophyll content and delivers an effective response verified in *Eucalyptus* species (Datt 1999) for being little affected by the interference caused by the scattering of radiation by the leaves, as well as by variations in internal structure (Pu et al. 2008). Such characteristics make it a potential index for forest vegetation approaches.

$$LCI = \frac{\rho 850nm - \rho 710nm}{\rho 850nm + \rho 680nm} \quad (9)$$

Wherein:

$\rho 850nm$: reflectance at 850 nanometers;
$\rho 710nm$: reflectance at 710 nanometers;
$\rho 680nm$: reflectance at 680 nanometers.

In an analogous way, the LWCI (*Leaf Water Content Index*) is correlated with leaf water content, and is based on one band in the near-infrared spectrum and another in the mid infrared region. The use of these bands is due to the spectral behavior of plant targets with the presence of water, where the LWCI represents the relative leaf water content – RWC (Raymond Hunt et al. 1987).

$$LWCI = \frac{\log(1-(\rho NIR - \rho MIDIR))}{-\log(1-\rho NIR - \rho MIDIR)} \quad (10)$$

Wherein:

ρNIR: reflectance in the near-infrared;
$\rho MIDIR$: reflectance in the mid-infrared.

Among the vegetation indices, indices based only on bands of the VIS electromagnetic spectrum provide a satisfactory response when accompanied by a classifier (Masemola et al. 2020). *Green Leaf Index* (GLI) is based on three VIS bands, and because it is based on the blue band, it has the atmospheric scattering effects attenuated, which proposes a different response than the other indices adopted in this study.

$$GLI = \frac{2\times\rho GREEN-\rho RED-\rho BLUE}{2\times\rho GREEN+\rho RED+\rho BLUE} \quad (11)$$

Wherein:

$\rho GREEN$: reflectance in the green;
ρRED: reflectance in the red;
$\rho BLUE$: reflectance in the blue.

2.6 Statistical Analyses

2.6.1 Principal Component Analysis

The datasets were submitted to Principal Component (PC) analysis by R software (R Development Core Team 2005), using 'ggfortify' (Tang et al. 2016) library. Hither, four data sets were established for PC analysis, with the first consisting of the representative bands and ranges (Table 1), the second being the RID values (Table 2), the third group consisting of the vegetation indices used, and a fourth group consisting of the means of the blue, green, red, and near-infrared wavelengths from the spectral curves of the samples. This fourth group was subjected to PC analysis with the other groups individually to verify the ability of the representative bands, RID values, and vegetation indices to discriminate native Amazonian Forest species and the relationship of each variable in each set to the species varieties.

2.6.2 Cluster analysis

As with PC analysis, for cluster analysis (CA), each data set must be analyzed in isolation. Ward's hierarchical agglomerative algorithm (Ward, 1963), whose measure of dissimilarity is the mean Euclidean distance, is given by Equation 12 (Everitt and Dunn 1991):

$$d_e = \left[\sum_{j=1}^{n}(P_{pj} - P_{kj})^2\right]^{\frac{1}{2}} \quad (12)$$

Wherein:

d_e is the Euclidean distance, and;

$P_{p,j}$ and $P_{k,j}$ are the j-variables of individuals p and k, respectively.

Ward's algorithm forms groups by minimizing dissimilarity or total sums of squares within groups, also known as the sum of squares of deviations (SQD). In each step of the procedure, groups are formed such that the resulting solution has the smallest SQD within groups. In these steps, joins of all possible pairs of groups are considered, and the two resulting in the smallest increase in SQD are grouped until all groups form a single one, gathering all individuals (Everitt and Dunn 1991; Torres et al. 2015).

Furthermore, d_M (Mahalanobis distance) makes it possible to quantify the relative contribution of the variables to the difference between Amazonian species in each dataset using the criteria proposed by Singh (1981), based on S_j statistics. In this case, we consider a Mahalanobis distance defined below (Equation 13).

$$d_M = \delta'_{ii'}\psi^{-1}\delta_{ii'}\sum_{j=1}^{p}\sum_{j'=1}^{p}\omega_{jj'}d_j d_{j'} \quad (15)$$

Wherein:

$\omega_{jj'}$ is the element of the jth row and j'-th inverse column of the matrix of residual variances and covariances.

The percentage values of S_j are the measure of the relative importance of variable j (from each data set) for the difference between the species, expressed by Equation 14.

$$S_j = \left(\frac{\sum_{j'=1}^{p}\omega_{jj'}d_{j'}d_j}{\sum_{j=1}^{p}S_j}\right)\times 100. \quad (14)$$

3. RESULTS

From FieldSpec® 4 data, the spectral curves of the evaluated plant species were created (Figure 5), and the vegetation indices were calculated for discriminatory analysis.

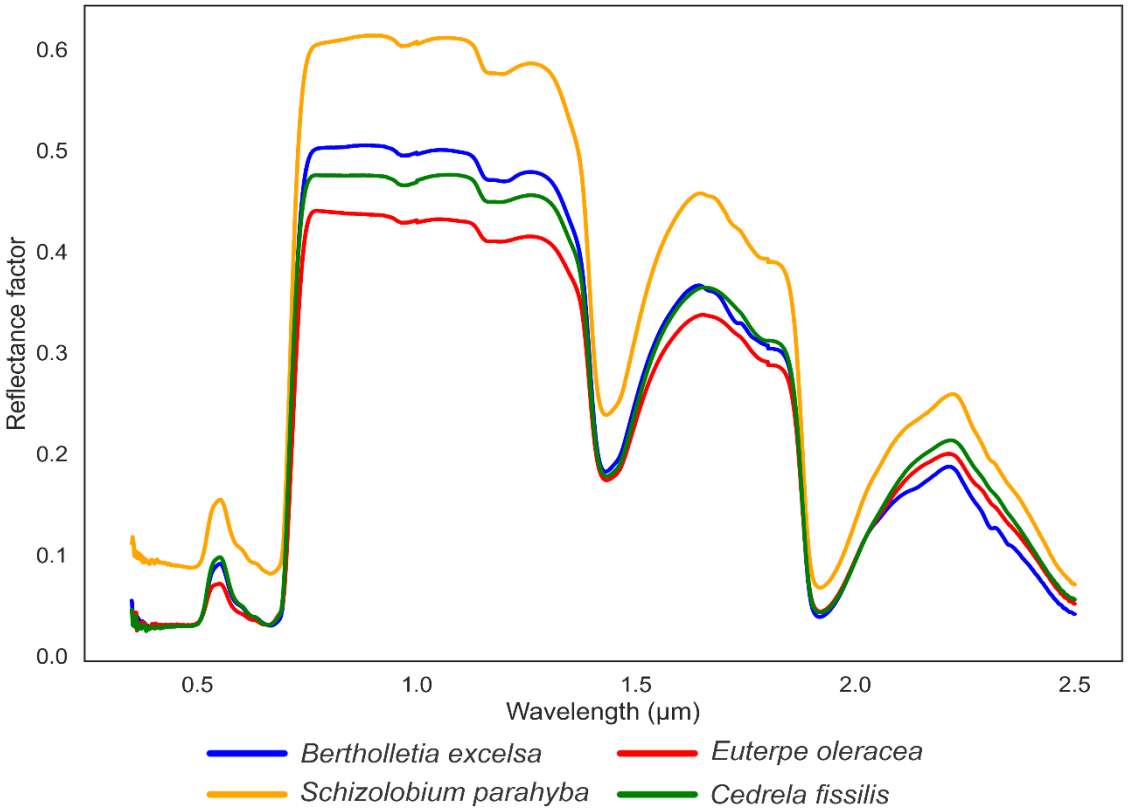

Figure 5. Spectral signature of the evaluated species, with the horizontal axis being the wavelength (µm) and the vertical axis being the percent reflectance.

By visual analysis, some regions of the electromagnetic spectrum with higher differentiation in reflectance responses can be seen, in portions of the visible spectrum (0.5 - 0.65 µm), near-infrared (0.913 – 1.25 µm) and SWIR 2 (2.1 – 2.5 µm), as highlighted in Figure 6. From the spectral library, the reflectance values for the 28 spectral intervals and inflection points representative of the biochemical composition at the leaf level were measured (Table 3).

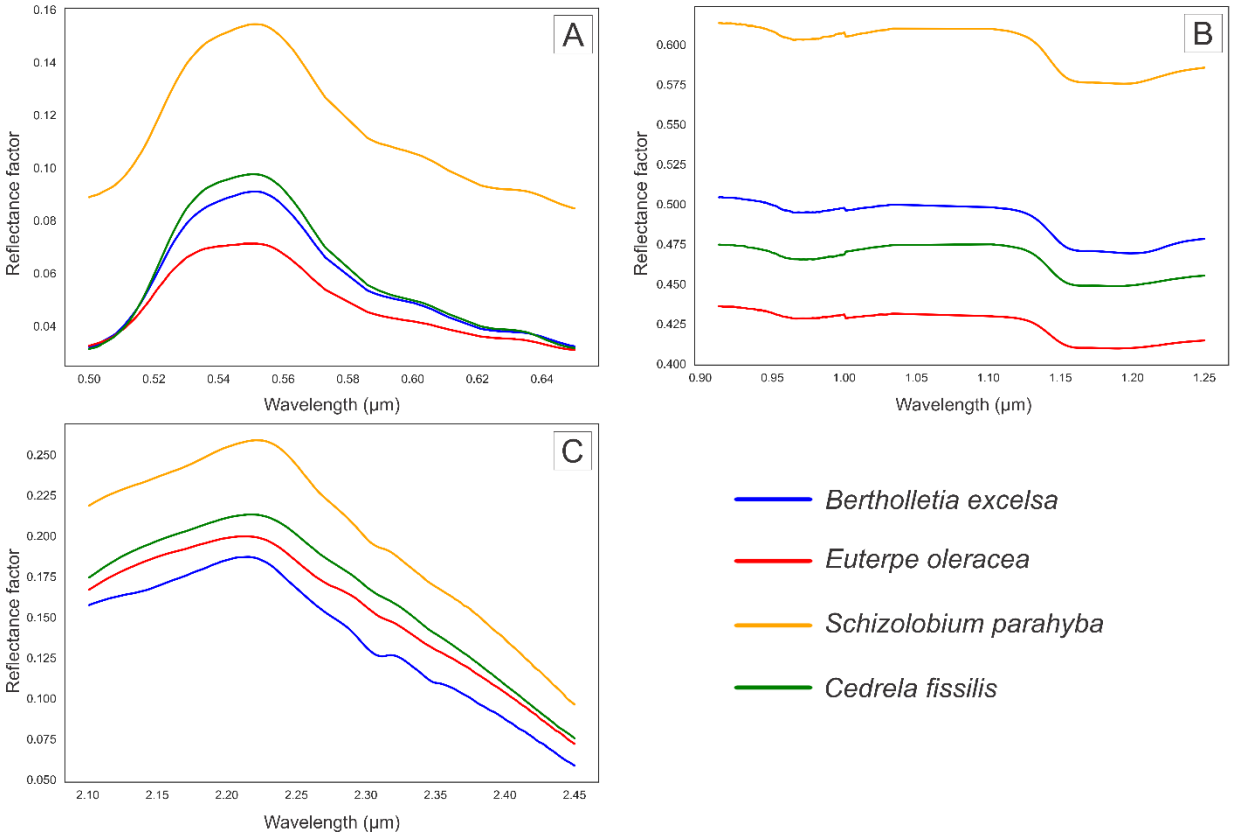

Figure 6. Spectral signature ranges with the highest difference between the reflectance values of the evaluated species, where A - visible spectrum; B - near-infrared, and C - SWIR 2.

Table 3. Reflectance factor in the spectral bands and inflection points representative of the leaf structure.

Band	*B. excelsa*	*E. oleracea*	*S. parahyba*	*C. fissilis*
1	0.0387883	0.0381901	0.0995234	0.0294417
2	0.0322674	0.0312767	0.0991512	0.0287680
3	0.0295023	0.0297905	0.0949492	0.0277122
4	0.0280561	0.0296431	0.0919339	0.0277269
5	0.0281852	0.0295000	0.0918993	0.0286455
6	0.0299413	0.0305933	0.0921771	0.0285859
7	0.0292421	0.0299946	0.0906873	0.0281718
8	0.0292437	0.0306887	0.0888572	0.0290923
9	0.0292980	0.0303981	0.0874105	0.0292866
10	0.0296961	0.0305054	0.0871209	0.0295904
11	0.0468631	0.0440066	0.1037252	0.0468178

12	0.0841212	0.0689784	0.1461410	0.0910710
13	0.0872634	0.0702222	0.1500176	0.0944742
14	0.0500768	0.0427238	0.1073540	0.0512034
15	0.0322656	0.0309660	0.0845492	0.0316428
16	0.0312670	0.0307002	0.0833196	0.0311421
17	0.0309623	0.0339717	0.0826009	0.0333111
18	0.0325463	0.0370830	0.0844210	0.0359054
19	0.0360263	0.0415363	0.0881747	0.0400615
20	0.0522007	0.0531267	0.1074606	0.0596333
21	0.1355049	0.1153380	0.2072679	0.1510268
22	0.1951492	0.1599440	0.2763079	0.2089977
23	0.3117758	0.2528179	0.4071327	0.3169921
24	0.4960168	0.4292705	0.6043329	0.4661718
25	0.4981131	0.4299003	0.6099862	0.4749999
26	0.2543505	0.2339375	0.3219815	0.2445984
27	0.0402941	0.0451426	0.0693014	0.0440182
28	0.1850987	0.1986600	0.2545797	0.2110869

The principal component (PC) analysis was performed three times with the four data sets, relative to the representative bands of leaf biochemistry (Table 1), RID intervals (Table 2), calculated vegetation indices, and the analyzed species to verify the association between the first three sets and the evaluated species, individually. It is evident that PC1 explained more than 99% of the variation in the three predictor data sets, as shown below.

The PC analysis application between the bands representing the leaf structure and the species showed the spectral intervals with the greatest contribution in distinguishing species, where the points closest to the species (represented by the red vectors) showed the highest contribution. Therefore, the bands contained in cluster 3 (22, 23, 26, and 28) were the most significant, as they were associated with the response of all four species (Figure 7A). The reflectance data at the representative spectral bands and points are presented in the heatmap (Figure 7B).

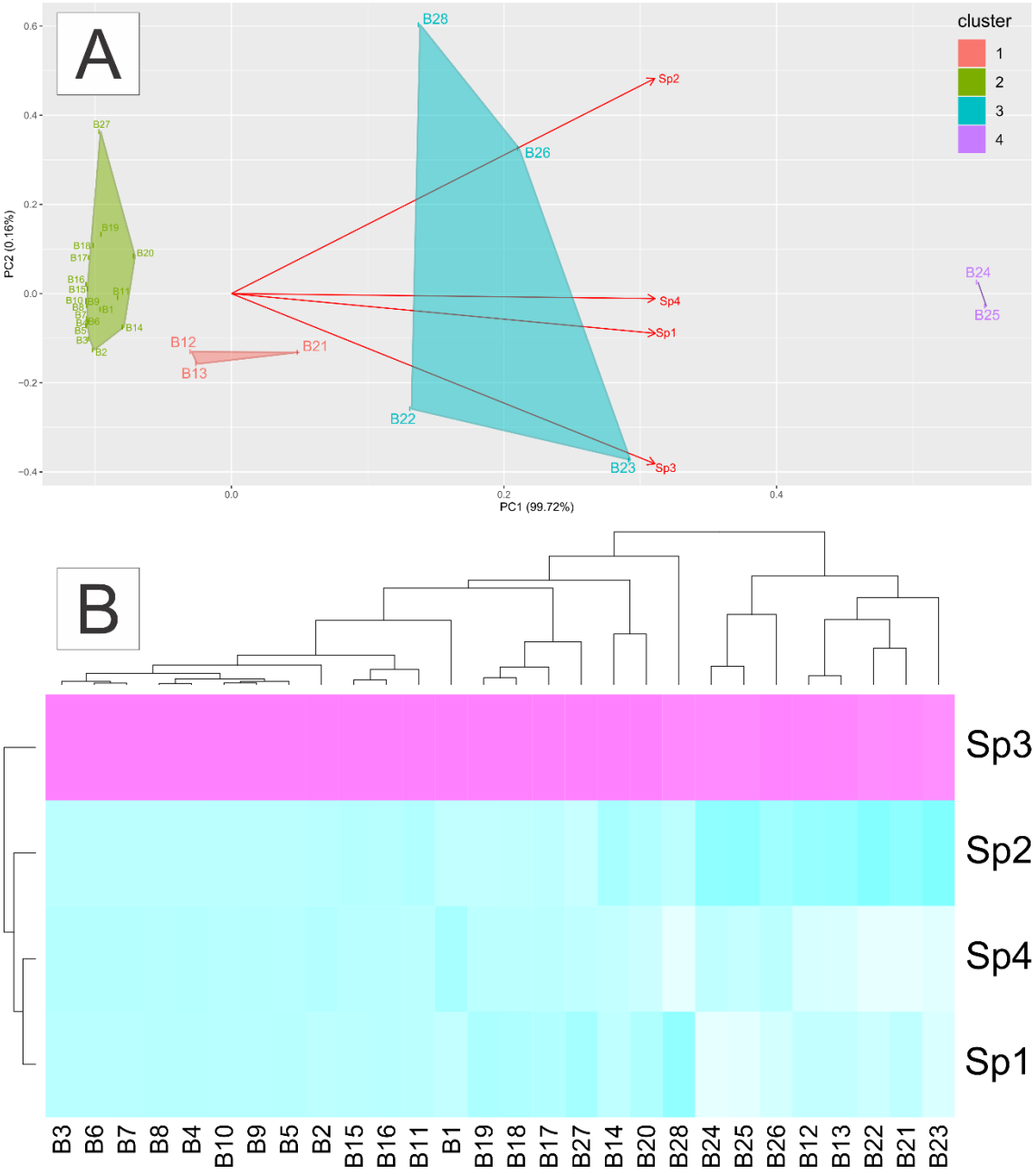

Figure 7. Graphical representation of the PC analysis with the data sets for the samples and the bands representing the leaf structure (A) and heatmap with the data sets for the samples and the bands representing the leaf structure (B), where: *Berthollethia excelsa* (Sp1), *Euterpe oleracea* (Sp2), *Schizolobium parahyba* (Sp3) and *Cedrela fissilis* (Sp4).

The differences between the maximum and minimum RID values at each height (ΔRID) were calculated, and it was noted that the response at heights 8 and 16 showed the highest difference (Table 4). In another perspective based on the RID

values, we observed that the values for *E. oleracea* were the lowest for 19 of the 22 intervals, while the values for *S. parahyba* were the highest for 17 intervals.

Table 4. RID values for each species and the difference between the highest and lowest value for each height.

Heigth	*B. excelsa*	*E. oleracea*	*S. parahyba*	*C. fissilis*	ΔRID
1	0.022708	0.01317	0.016163	0.0156	0.009538123
2	0.002101	0.004257	0.001766	0.001317	0.002940598
3	0.049273	0.035232	0.051666	0.054918	0.019685268
4	0.005615	0.003004	0.007194	0.006779	0.004190191
5	0.021309	0.016498	0.023401	0.024724	0.008226542
6	0.0101	0.006596	0.012357	0.011025	0.005760696
7	0.007035	0.005189	0.00925	0.00847	0.004060973
8	0.464203	0.403087	0.515404	0.440853	0.112316481
9	0.004134	0.003457	0.009846	2.85E-05	0.009817678
10	0.003949	0.003488	0.004229	0.003907	0.000741359
11	0.004966	0.003569	0.005126	0.004381	0.001557679
12	0.00116	0.000811	0.001255	0.000953	0.000443393
13	0.003025	0.001448	0.004283	0.00722	0.005771891
14	0.027352	0.019866	0.033657	0.025856	0.013791078
15	0.008652	0.005064	0.010083	0.006826	0.005018609
16	0.295556	0.239821	0.346429	0.276532	0.10660753
17	0.183155	0.160739	0.2169	0.182746	0.05616141
18	0.05715	0.045781	0.064197	0.05207	0.018415794
19	0.263666	0.241482	0.319873	0.266655	0.078390097
20	0.112918	0.121815	0.146602	0.131795	0.033683426
21	0.023567	0.021595	0.028576	0.025345	0.006981319
22	0.128508	0.127706	0.162094	0.137679	0.034387526

ΔRID: difference between the highest and lowest RID value for each height

There was a higher contribution in distinguishing between species based on RID heights 8, 16, and 19 (Figure 8A), contained in the first cluster. The direction of

the vectors associated with the species motivates the high variability in the direction of the PC1 axis. Based on these data sets, the heatmap (Figure 8B) was also prepared, scaled according to the values present in Table 4, where the highest values are represented by pink color and the lowest by blue color.

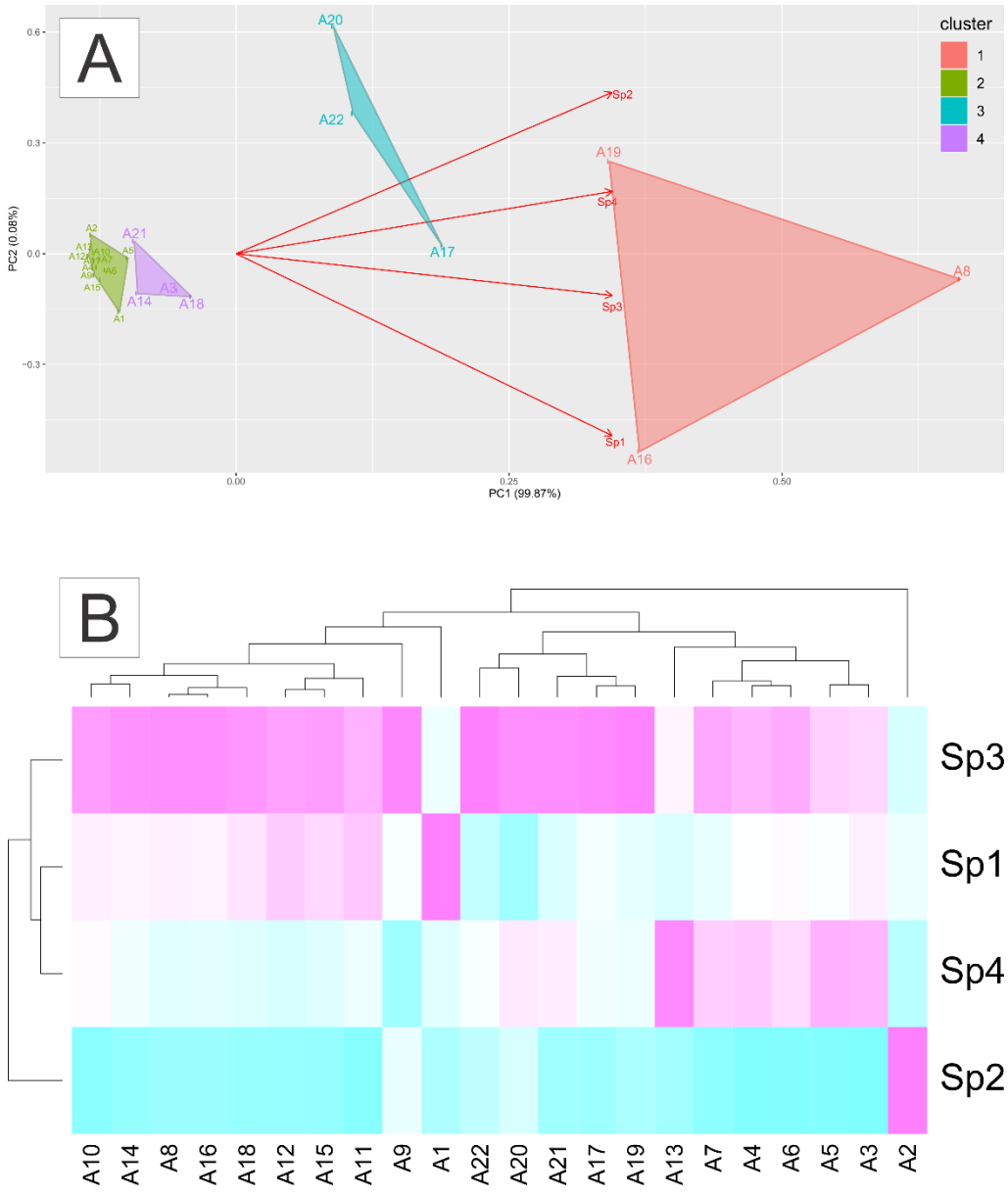

Figure 8. Graphical representation of PC analysis with the data sets for the samples and RID intervals (A) and heatmap with the data sets for the samples and RID intervals (B), where: *Bertholletia excelsa* (Sp1), *Euterpe oleracea* (Sp2), *Schizolobium parahyba* (Sp3), and *Cedrela fissilis* (Sp4).

For the PC analysis applied to the vegetation indices, it was possible to observe that the NPCI, TVI, and CARI2 indices contained in cluster 1 were those

closest to the species vectors (Figure 9A). Among them, Singh's criterion (1981) reveals that the CARI2 and NPCI indices accounted for 70.45% and 16.73% of the differentiation of the evaluated species, respectively (Table 5). From a graphical representation perspective, the heatmap (Figure 9B) was elaborated to visualize the vegetation indices regarding to the analyzed species. In this figure, higher values are represented by pink and lower values are represented by blue color.

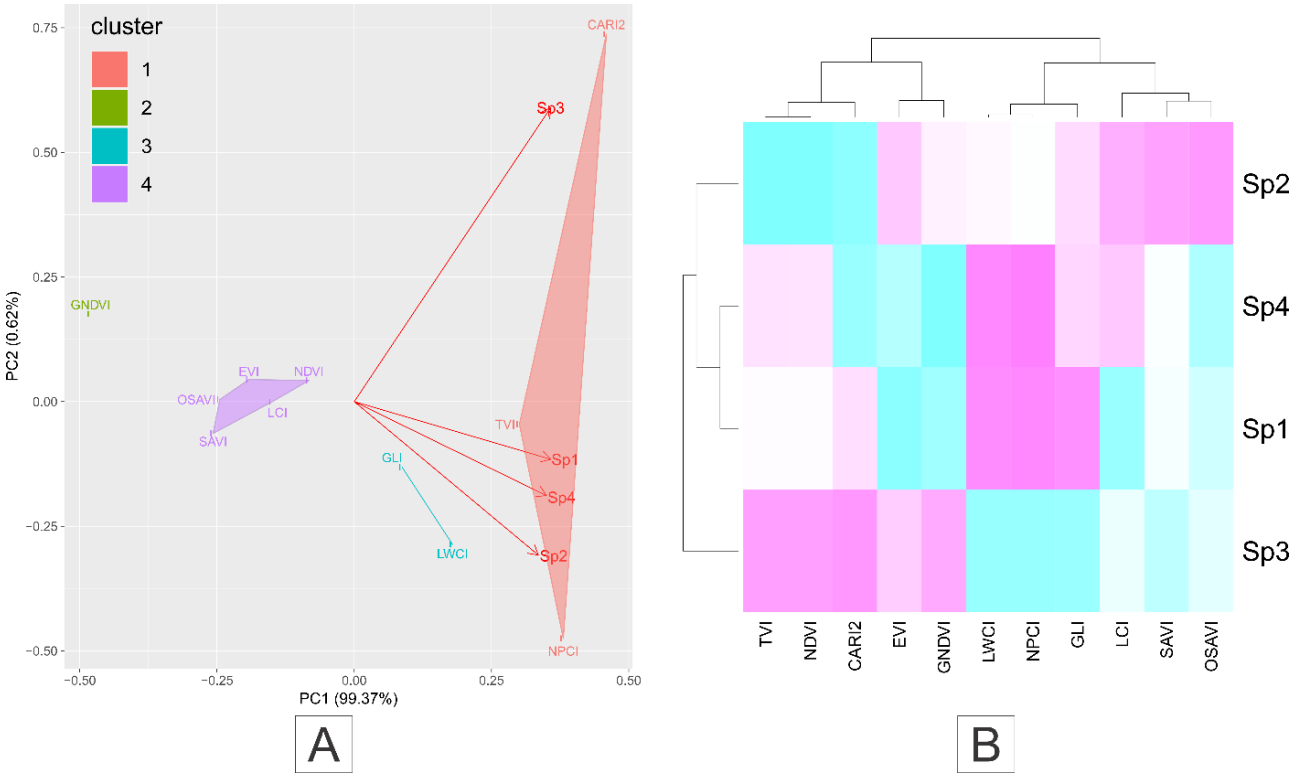

Figure 9. Graphical representation of PC analysis with sample and vegetation index datasets (A) and heatmap with sample and vegetation index datasets (B), where: *Bertholletia excelsa* (Sp1), *Euterpe oleracea* (Sp2), *Schizolobium parahyba* (Sp3), and *Cedrela fissilis* (Sp4).

Euterpe oleracea had the highest values for LCI, SAVI, GLI and OSAVI. The species *Bertholletia excelsa* and *Cedrela fissilis* showed similar values for EVI, GNDVI, LWCI, and NPCI. On the other hand, the samples of *Schizolobium parahyba* reached the highest values for the TVI, NDVI, CARI2, and GNDVI indices. By Singh's criterion, the relative contributions (Sj) of each vegetation index evaluated for distinction can be verified, as well as their percentage values (Table 5).

Table 5. Vegetative characteristics and their centered spectral responses.

Vegetation Index	S_j	Percentage Value (%)
EVI	0.000593	0.17
NDVI	0.000393	0.11
GNDVI	0.006261	1.76
SAVI	0.007144	2.01
TVI	0.000207	0.06
OSAVI	0.002625	0.74
NPCI	0.059369	16.73
CARI2	0.250080	70.45
LCI	0.001586	0.45
LWCI	0.022424	6.32
GLI	0.004288	1.21

4. DISCUSSION

Based on the spectral curves obtained, the reflectance characteristics between species occurring in a native environment can be compared, where trees with a sunlit canopy show a higher difference between NIR and SWIR reflectance factors than species with a shade canopy), followed by species with medium height (Wu et al. 2017). This response is evident when comparing the curves of *C. fissilis* and *B. excelsa*, with shade (Carvalho 2005) and sunlit canopy (Corrêa 1926; Salomão 2009), respectively, as seen in Figure 6B and 6C. It is noteworthy that leaf morphology has no significant impact on the leaf-based spectrum, where the spectral behavior suggests a substantial similarity between *E. oleracea* and *C. fissilis*, in which the first is a palm tree with long and narrow folioles, and the second is a woody tree with short and wide folioles (Martins da Silva et al. 2014).

Looking at biochemical characteristics associated with the reflectance factor at specific wavelengths, the chlorophyll absorption characteristic at 550 nanometers was not significant in differentiating, as the responses for the four species were quite close. Conversely, the behavior in the red-edge region

(represented by bands 22 and 23 in the representative bands approach) allowed for differentiation with greater importance, which is supported by the PC analysis results. The red-edge region in the electromagnetic spectrum relates to light scattering in the mesophyll and interacts with the internal leaf structure (Sánchez-Azofeifa et al. 2009). Taking the distinction between species as an objective, the bands described in cluster 3 in Figure 7A are arranged in positions of high reflectance variation, indicating that higher reflectance variability is essential for good results in species identification. (Miyoshi et al. 2020). The importance of bands 22 and 23 in this model relates to the red-edge region of the spectrum, which varies with nitrogen and chlorophyll content, making it important in differentiating between plants (Flores et al., 2020; Liu et al., 2021; Peñuelas et al., 1994). Furthermore, the variability described by PC1 being very close to the total data variability (99.72%) suggests that the differentiation between species by representative bands approach is effective.

Following the model for estimating anthocyanin uptake (Sims and Gamon 2002), it was found that the highest absorbance for this component occurred in the samples of *S. parahyba* and was similar for the other species evaluated. This condition is noted by the leaf coloration of the species evaluated since this model is based on visible wavelengths. Furthermore, the heatmap in Figure 7B reinforces this result since *S. parahyba* presents higher reflectance throughout the measured spectrum.

The RID approach quantified the difference between the maximum and minimum inflection intervals (RID) for the 22 heights (Nanni et al. 2004) and detailed spectral signature. The RID comparison with the highest difference at heights 8 and 16 suggests that these spectral ranges are relevant in differentiating plant species, which is evidenced by the PC analysis. Similar to the response of PC analysis with data from representative bands, the RID approach proved to be efficient in characterizing the spectral curve from the standpoint of data variability, with almost its entirety at PC1 (99.87%). From a leaf biochemistry perspective, if we compile the results from the RID intervals in the visible region with the spectral curve obtained, we note that the chlorophyll content (Lichtenthaler et al. 1998) in *E. oleracea* naturally is higher than the other species evaluated.

The application of vegetation spectral models was intended to summarize the spectral curve response to a mathematical value and become a tool for discriminant analysis. It is notable that vegetation indices have become effective in applications with hyperspectral data (Silva Junior et al. 2018) compared to notable research from decades past (Asner et al. 2008). The PC analysis applied to the vegetation spectral models brought satisfactory results, with PC1 highly related to the variability of the vegetation indices results (99.37%). Adopting this approach in hyperspectral data at the leaf level and well-defined classes results in good responses (Kalacska et al. 2007; Silva Junior et al. 2018). We emphasize the importance of using combined vegetation indices, with greater contributions by indices developed for quantization (NPCI) or absorption of electromagnetic radiation by chlorophyll (CARI2), which are based in the visible region.

5. CONCLUSIONS

The analysis of spectral curves of plant species allows their characterization based on several key reflectance points. The approaches of representative bands, RID and vegetation spectral models subjected to principal component analysis show significant contribution in the distinction, highlighting representative bands and RID intervals with higher reflectance variation, as well as vegetation indices related to the interaction of chlorophyll with radiation in the visible region. The methodology applied based on the spectral libraries generated for each plant was effective, proving to be a successful model in distinguishing plant species through spectroradiometry. Based on the spectral curves obtained here, future works using hyperspectral remote sensing in floristics and species conservation will be feasible.

6. ACKNOWLEDGEMENTS

This study was financed in part by the Coordenação de Aperfeiçoamento de Pessoal de Nível Superior - Brasil (CAPES) - Finance Code 001, National Council for Research and Development (CNPq). We are also thanking to the research laboratories of State University of Mato Grosso (UNEMAT). This is a research derived from the first author's degree in the Graduate Program in Environmental Sciences (PPGCAM) at Federal University of Mato Grosso (UFMT).

7. REFERENCES

Alvares, C. A., Stape, J. L., Sentelhas, P. C., Gonçalves, J. L. de M., Sparovek, G., & others. (2013). Köppen's climate classification map for Brazil. *Meteorologische Zeitschrift*, *22*(6), 711–728.

Asner, G. P., Knapp, D. E., Kennedy-Bowdoin, T., Jones, M. O., Martin, R. E., Boardman, J., & Hughes, R. F. (2008). Invasive species detection in Hawaiian rainforests using airborne imaging spectroscopy and LiDAR. *Remote Sensing of Environment*, *112*(5), 1942–1955. https://doi.org/10.1016/j.rse.2007.11.016

Baldeck, C. A., Asner, G. P., Martin, R. E., Anderson, C. B., Knapp, D. E., Kellner, J. R., & Wright, S. J. (2015). Operational tree species mapping in a diverse tropical forest with airborne imaging spectroscopy. *PLoS ONE*, *10*(7). https://doi.org/10.1371/journal.pone.0118403

Balzon, D. R., Silva, J. C. G. L. da, & Santos, A. J. dos. (2004). Aspectos Mercadológicos De Produtos Florestais Não Madeireiros – Análise Retrospectiva. *Floresta*, *34*(3), 363–371. https://doi.org/10.5380/rf.v34i3.2422

Brandelero, C., Berra, E. F., Backes, K. S., Pereira, R. S., & Brun, E. J. (2012). Espectrorradiometria na região do visível e do infravermelho próximo em povoamento de Eucalyptus grandis Hill ex Maiden. *Ciência Florestal*, *22*(1). https://doi.org/10.5902/198050985093

Brandes, A. F. das N., Novello, B. Q., Domingues, G. de A. F., Barros, C. F., & Tamaio, N. (2020). Endangered species account for 10% of Brazil's documented timber trade. *Journal for Nature Conservation*, *55*(March), 125821. https://doi.org/10.1016/j.jnc.2020.125821

Brito, M. M. de, & Farias, A. (2013). Espectroradiometria foliar de árvores frutíferas e o efeito da umidade sobre a resposta espectral das folhas. In *XVI Simpósio Brasileiro de Sensoriamento Remoto* (pp. 3245–3252). Foz do Iguaçu: INPE. http://marte2.sid.inpe.br/col/dpi.inpe.br/marte2/2013/05.29.00.17.23/doc/p1012.pdf

Broge, N., & Leblanc, E. (2001). Comparing prediction power and stability of broadband and hyperspectral vegetation indices for estimation of green leaf area index and canopy chlorophyll density. *Remote Sensing of Environment*, *76*, 156–172. https://doi.org/10.1016/S0034-4257(00)00197-8

Cardoso, D., Särkinen, T., Alexander, S., Amorim, A. M., Bittrich, V., Celis, M., et al.

(2017). Amazon plant diversity revealed by a taxonomically verified species list. *Proceedings of the National Academy of Sciences*, *114*(40), 10695–10700. https://doi.org/10.1073/pnas.1706756114

Carvalho, P. E. R. (2005). Cedro. *Embrapa Florestas-Circular Técnica (INFOTECA-E)*.

Catinon, M., Ayrault, S., Boudouma, O., Asta, J., Tissut, M., & Ravanel, P. (2009). The inclusion of atmospheric particles into the bark suber of ash trees. *Chemosphere*, *77*(10), 1313–1320. https://doi.org/https://doi.org/10.1016/j.chemosphere.2009.09.039

Caturegli, L., Lulli, F., Foschi, L., Guglielminetti, L., Bonari, E., & Volterrani, M. (2014). Monitoring turfgrass species and cultivars by spectral reflectance. *European Journal of Horticultural Science*, *79*(3), 97–107.

Chatziantoniou, A., Petropoulos, G. P., & Psomiadis, E. (2017). Co-Orbital Sentinel 1 and 2 for LULC mapping with emphasis on wetlands in a mediterranean setting based on machine learning. *Remote Sensing*, *9*(12). https://doi.org/10.3390/rs9121259

Chavana-Bryant, C., Malhi, Y., Anastasiou, A., Enquist, B. J., Cosio, E. G., Keenan, T. F., & Gerard, F. F. (2019). Leaf age effects on the spectral predictability of leaf traits in Amazonian canopy trees. *Science of the Total Environment*, *666*, 1301–1315. https://doi.org/10.1016/j.scitotenv.2019.01.379

Chicati, M. L. (2011). *Avaliação espectral de solos em áreas alagáveis do noroeste do Paraná*. Universidade Estadual de Maringá. Retrieved from http://repositorio.uem.br:8080/jspui/bitstream/1/1110/1/000189040.pdf

Clark, M. L., Roberts, D. A., & Clark, D. B. (2005). Hyperspectral discrimination of tropical rain forest tree species at leaf to crown scales. *Remote Sensing of Environment*, *96*(3–4), 375–398. https://doi.org/10.1016/j.rse.2005.03.009

Clevers, J. G. P. W., Kooistra, L., & Schaepman, M. E. (2008). Using spectral information from the NIR water absorption features for the retrieval of canopy water content. *International Journal of Applied Earth Observation and Geoinformation*, *10*(3), 388–397. https://doi.org/https://doi.org/10.1016/j.jag.2008.03.003

Clevers, J. G. P. W., Kooistra, L., & Schaepman, M. E. (2010). Estimating canopy water content using hyperspectral remote sensing data. *International Journal of Applied Earth Observation and Geoinformation*, *12*(2), 119–125.

https://doi.org/10.1016/j.jag.2010.01.007

Cohen, W. B., & Justice, C. O. (1999). Validating MODIS Terrestrial Ecology Products. *Remote Sensing of Environment*, *70*(1), 1–3. https://doi.org/10.1016/s0034-4257(99)00053-x

Corrêa, M. P. (1926). Diccionário das plantas úteis do Brasil e das exóticas cultivadas. In *Diccionario das plantas uteis do Brasil e das exoticas cultivadas* (p. 747).

Crusiol, L G T, Nanni, M. R., Furlanetto, R. H., Cezar, E., Sibaldelli, R. N. R., Mertz-Henning, L. M., et al. (2019). Obtenção de assinatura espectral de cultivares de soja. In *37ª Reunião de Pesquisa de Soja* (pp. 25–28). Londrina: Comissão de Ecologia, Fisiologia e Práticas Culturais. https://www.alice.cnptia.embrapa.br/bitstream/doc/1110936/1/25.pdf

Crusiol, Luís Guilherme Teixeira, Nanni, M. R., Furlanetto, R. H., Sibaldelli, R. N. R., Cezar, E., Sun, L., et al. (2021). Yield prediction in soybean crop grown under different levels of water availability using reflectance spectroscopy and partial least squares regression. *Remote Sensing*, *13*(5), 1–21. https://doi.org/10.3390/rs13050977

Daljit Singh. (1981). The relative importance of characters affecting genetic divergence. *Indian Journal of Genetics and Plant Breeding*, *41*, 237–245.

Datt, B. (1999). A new reflectance index for remote sensing of chlorophyll content in higher plants: Tests using Eucalyptus leaves. *Journal of Plant Physiology*, *154*(1), 30–36. https://doi.org/10.1016/S0176-1617(99)80314-9

Dong, X., Lu, X., Wu, X., Liu, G., Yan, L., Muhammad, R., et al. (2018). Changes in chemical composition and structure of root cell wall of citrus rootstock seedlings in response to boron deficiency by FTIR spectroscopy. *Journal of Horticultural Science and Biotechnology*, *93*(2), 150–158. https://doi.org/10.1080/14620316.2017.1362327

Ellenberg, D., & Mueller-Dombois, D. (1974). *Aims and methods of vegetation ecology*. Wiley New York.

Everitt, B., & Dunn, G. (1991). *Applied multivariate data analysis / Brian S. Everitt and Graham Dunn*. London ; Melbourne: Edward Arnold.

Feeley, K. J., & Silman, M. R. (2009). Extinction risks of Amazonian plant species. *Proceedings of the National Academy of Sciences*, *106*(30), 12382–12387. https://doi.org/10.1073/pnas.0900698106

Feeley, K. J., & Silman, M. R. (2011). Keep collecting: accurate species distribution modelling requires more collections than previously thought. *Diversity and Distributions*, *17*(6), 1132–1140. https://doi.org/https://doi.org/10.1111/j.1472-4642.2011.00813.x

Felfili, Jeanine Maria, Roitman, I., Medeiros, M. M., & Sanchez, M. (2011). Procedimentos e métodos de amostragem de vegetação. In J. M (Ed.), *Fitossociologia no Brasil: métodos e estudos de caso.* (1st ed., pp. 86–121). Viçosa: Editora da Universidade Federal de Viçosa.

Filella, I., & Peñuelas, J. (1994). The red edge position and shape as indicators of plant chlorophyll content, biomass and hydric status. *International Journal of Remote Sensing*, *15*(7), 1459–1470. https://doi.org/10.1080/01431169408954177

Filella, I., Serrano, L., Serra, J., & Peñuelas, J. (1995). Evaluating Wheat Nitrogen Status with Canopy Reflectance Indices and Discriminant Analysis. *Crop Science*, *35*(5), 1400–1405. https://doi.org/10.2135/cropsci1995.0011183x003500050023x

Filgueiras, T. S., Nogueira, P. E., Brochado, A. L., Guala, G. F., & others. (1994). Caminhamento: um método expedito para levantamentos florísticos qualitativos. *Cadernos de Geociências*, *12*(1), 39–43.

Fiorio, P. R., Demattê, J. A. M., Nanni, M. R., & Formaggio, A. R. (2010). Diferenciação espectral de solos utilizando dados obtidos em laboratório e por sensor orbital. *Bragantia*, *69*(2), 453–466. https://doi.org/10.1590/s0006-87052010000200025

Flores, M. S., Paschoalete, W. M., Baio, F. H. R., Campos, C. N. S., Pantaleão, A. de A., Teodoro, L. P. R., et al. (2020). Relationship between vegetation indices and agronomic performance of maize varieties under different nitrogen rates. *Bioscience Journal*, *36*(5), 1638–1644. https://doi.org/10.14393/BJ-v36n5a2020-47993

Flores, T. B. (2020). Meliaceae in Flora do Brasil 2020. *Jardim Botânico do Rio de Janeiro*. http://floradobrasil.jbrj.gov.br/reflora/floradobrasil/FB9990. Accessed 9 June 2021

Fu, Y., Hou, M., Zang, H., Li, H., Chin, S. L., & Xu, H. (2019). Remote discrimination of willow, pine and poplar trees and their growing environments by femtosecond

filament-induced breakdown spectroscopy. *Spectrochimica Acta Part B: Atomic Spectroscopy*, *155*, 107–114. https://doi.org/https://doi.org/10.1016/j.sab.2019.04.001

Furlanetto, R. H., Moriwaki, T., Falcioni, R., Pattaro, M., Vollmann, A., Sturion Junior, A. C., et al. (2020). Hyperspectral reflectance imaging to classify lettuce varieties by optimum selected wavelengths and linear discriminant analysis. *Remote Sensing Applications: Society and Environment*, *20*(May), 100400. https://doi.org/10.1016/j.rsase.2020.100400

Gitelson, A. A., Kaufman, Y. J., & Merzlyak, M. N. (1996). Use of a green channel in remote sensing of global vegetation from EOS-MODIS. *Remote Sensing of Environment*, *58*(3), 289–298. https://doi.org/https://doi.org/10.1016/S0034-4257(96)00072-7

Gomes, L., Nobre, T., Sousa, A., Rei, F., & Guiomar, N. (2020). Hyperspectral reflectance as a basis to discriminate olive varieties-A tool for sustainable crop management. *Sustainability (Switzerland)*, *12*(7), 1–21. https://doi.org/10.3390/su12073059

Grings, M., & Brack, P. (2011). Cedrela fissilis. In L. Coradin, A. Siminski, & A. Reis (Eds.), *Espécies nativas da flora brasileira de valor econômico atual ou potencial: plantas para o futuro – Região Sul* (pp. 444–447). Brasília: Ministério do Meio Ambiente.

Guzmán Q., J. A., Rivard, B., & Sánchez-Azofeifa, G. A. (2018). Discrimination of liana and tree leaves from a Neotropical Dry Forest using visible-near infrared and longwave infrared reflectance spectra. *Remote Sensing of Environment*, *219*, 135–144. https://doi.org/https://doi.org/10.1016/j.rse.2018.10.014

Henderson, A., & Galeano, G. (1996). Euterpe, Prestoea, and Neonicholsonia (Palmae). *Flora Neotropica*, *72*, 1–89. http://www.jstor.org/stable/4393873

Homma, A. K. O. (2011a). Biodiversidade e biopirataria na Amazônia: como reduzir os riscos? *Passages de Paris*, *6*, 111–128. https://www.alice.cnptia.embrapa.br/alice/bitstream/doc/954896/1/PP6artigo4.pdf

Homma, A. K. O. (2011b). Madeira na Amazônia: extração, manejo ou reflorestamento? *Amazônia: Ciência & Desenvolvimento*, *7*(13), 147–162. http://www.alice.cnptia.embrapa.br/handle/doc/944362

Huete, A. R., Liu, H. Q., Batchily, K., & Leeuwen, W. Van. (1997). A comparison of vegetation indices over a global set of TM images for EOS-MODIS. *Remote Sensing of Environment*, *59*(3), 440–451. https://doi.org/10.1016/s0034-4257(96)00112-5

Jacquemoud, S., & Baret, F. (1990). PROSPECT: A model of leaf optical properties spectra. *Remote Sensing of Environment*, *34*(2), 75–91. https://doi.org/https://doi.org/10.1016/0034-4257(90)90100-Z

Janta, R., Chantara, S., Inta, A., Kawashima, M., & Satake, K. (2016). Levels of Road Traffic Heavy Metals in Tree Bark Layers of Cassia fistula Tree. *International Journal of Environmental Science and Development*, *7*(5), 385–388. https://doi.org/10.7763/ijesd.2016.v7.805

Jensen, J. (2007). *Remote sensing of the environment : an earth resource perspective*. Upper Saddle River, NJ: Pearson Prentice Hall.

Jensen, J. R. (2009). *Sensoriamento remoto do ambiente: uma perspectiva em recursos terrestres*. (J. C. N. EPIPHANIO, A. R. FORMAGGIO, A. R. DOS SANTOS, B. F. T. RUDORFF, C. M. DE ALMEIDA, & L. S. GALVÃO, Eds.) (2nd ed.). São José dos Campos: Parêntese. http://www.parentese.com.br/pdf/jensen.pdf

Kalacska, M., Bohlman, S., Sanchez-azofeifa, G. A., Castro-esau, K., & Caelli, T. (2007). Hyperspectral discrimination of tropical dry forest lianas and trees : Comparative data reduction approaches at the leaf and canopy levels, *109*, 406–415. https://doi.org/10.1016/j.rse.2007.01.012

Kersten, R. de A., & Galvão, F. (2011). Suficiência amostral em inventários florísticos e fitossociológicos. In Jeanini Maria Felfili, P. V. Eisenlorh, M. M. da R. F. de Melo, L. A. de Andrade, & J. A. A. M. Neto (Eds.), *Fitossociologia no Brasil: métodos e estudos de caso.* (pp. 156–173). Viçosa: Editora da Universidade Federal de Viçosa. https://doi.org/10.13140/2.1.2869.1524

Kim, M. S. (1994). *The use of narrow spectral bands for improving remote sensing estimations of fractionally absorbed photosynthetically active radiation (fAPAR)*. University of Maryland. Retrieved from https://doi.org/10.13016/tiej-8hku

Kishore, B. S. P. C., Kumar, A., Saikia, P., Lele, N., Pandey, A. C., Srivastava, P., et al. (2020). Major forests and plant species discrimination in Mudumalai forest region using airborne hyperspectral sensing. *Journal of Asia-Pacific Biodiversity*, *13*(4), 637–651. https://doi.org/10.1016/j.japb.2020.07.001

Lang, C., Costa, F. R. C., Camargo, J. L. C., Durgante, F. M., & Vicentini, A. (2015). Near infrared spectroscopy facilitates rapid identification of both young and mature Amazonian tree species. *PLoS ONE*, *10*(8), 1–15. https://doi.org/10.1371/journal.pone.0134521

Lichtenthaler, H., Wenzel, O., Bushman, C., & Gitelson, A. (1998). Plant Stress Detection by Reflectance and Fluorescencea. *Annals of the New York Academy of Sciences*, *851*(1), 271–285. https://doi.org/10.1111/j.1749-6632.1998.tb09002.x

Liu, E., Zhao, H., Zhang, S., He, J., Yang, X., & Xiao, X. (2021). Identification of plant species in an alpine steppe of Northern Tibet using close-range hyperspectral imagery. *Ecological Informatics*, *61*(9). https://doi.org/10.1016/j.ecoinf.2021.101213

Malvern Panalytical. (2019). Asd Fieldspec® 4. Malvern: Malvern Panalytical. https://www.malvernpanalytical.com/en/products/product-range/asd-range/fieldspec-range/fieldspec4-hi-res-high-resolution-spectroradiometer?campaignid=1564620399&adgroupid=69609821667&creative=332029566126&keyword=&matchtype=b&network=g&device=c&gclid=EAIa

Marshak, A., & Knyazikhin, Y. (2017). The spectral invariant approximation within canopy radiative transfer to support the use of the {EPIC}/{DSCOVR} oxygen B-band for monitoring vegetation. *Journal of Quantitative Spectroscopy and Radiative Transfer*, *191*, 7–12. https://doi.org/10.1016/j.jqsrt.2017.01.015

Martinelli, G., & Moraes, M. A. (2013). *Livro vermelho da flora do Brasil*. (G. Martinelli & M. A. Moraes, Eds.) (1st ed.). Rio de Janeiro: CNCFlora. https://www.researchgate.net/profile/Marcelo_Menezes2/publication/273000307_Cactaceae/links/54f48fca0cf2f28c1361e233.pdf

Martins da Silva, R. C. V., Silva, A. S. L. da, Fernandes, M. M., & Margalho, L. F. (2014). *Noções Morfológicas e Taxonômicas para Identificação Botânica*. *Embrapa* (1st ed.). Brasília: Embrapa. http://www.embrapa.br/amazonia-oriental/publicacoes

Masemola, C., Cho, M. A., & Ramoelo, A. (2020). Sentinel-2 time series based optimal features and time window for mapping invasive Australian native Acacia species in KwaZulu Natal, South Africa. *International Journal of Applied Earth*

Observation and Geoinformation, *93*(April), 102207. https://doi.org/10.1016/j.jag.2020.102207

Miyoshi, G. T., Imai, N. N., Tommaselli, A. M. G., de Moraes, M. V. A., & Honkavaara, E. (2020). Evaluation of hyperspectral multitemporal information to improve tree species identification in the highly diverse atlantic forest. *Remote Sensing*, *12*(2), 1–21. https://doi.org/10.3390/rs12020244

Morrison, D. F. (1976). *Multivariate statistical methods* (2nd ed.). Singapore: McGraw Hill.

Mudereri, B. T., Dube, T., Niassy, S., Kimathi, E., Landmann, T., Khan, Z., & Abdel-Rahman, E. M. (2020). Is it possible to discern Striga weed (Striga hermonthica) infestation levels in maize agro-ecological systems using in-situ spectroscopy? *International Journal of Applied Earth Observation and Geoinformation*, *85*, 102008. https://doi.org/https://doi.org/10.1016/j.jag.2019.102008

Nanni, M. R., & Dematte, J. A. M. (2000). *Dados radiométricos obtidos em laboratório e no nível orbital na caracterização e mapeamento de solos*. Universidade de São Paulo.

Nanni, M. R., Demattê, J. A. M., & Fiorio, P. R. (2004). Análise discriminante dos solos por meio da resposta espectral no nível terrestre. *Pesquisa Agropecuária Brasileira*, *39*(10), 995–1006. https://doi.org/10.1590/s0100-204x2004001000007

Nidamanuri, R. R. (2020). Hyperspectral discrimination of tea plant varieties using machine learning, and spectral matching methods. *Remote Sensing Applications: Society and Environment*, *19*, 100350. https://doi.org/https://doi.org/10.1016/j.rsase.2020.100350

Peng, D., Wang, Y., Xian, G., Huete, A. R., Huang, W., Shen, M., et al. (2021). Investigation of land surface phenology detections in shrublands using multiple scale satellite data. *Remote Sensing of Environment*, *252*(October 2020). https://doi.org/10.1016/j.rse.2020.112133

Peñuelas, J., Gamon, J. A., Fredeen, A. L., Merino, J., & Field, C. B. (1994). Reflectance indices associated with physiological changes in nitrogen- and water-limited sunflower leaves. *Remote Sensing of Environment*, *48*(2), 135–146. https://doi.org/https://doi.org/10.1016/0034-4257(94)90136-8

Ponzoni, F. J., & Shimabukuro, Y. E. (2009). *Sensoriamento remoto no estudo da*

vegetação. São José dos Campos: Parêntese Editora.

Pu, R., Gong, P., & Yu, Q. (2008). Comparative analysis of EO-1 ALI and Hyperion, and Landsat ETM+ data for mapping forest crown closure and leaf area index. *Sensors*, *8*(6), 3744–3766. https://doi.org/10.3390/s8063744

Raymond Hunt, E., Rock, B. N., & Nobel, P. S. (1987). Measurement of leaf relative water content by infrared reflectance. *Remote Sensing of Environment*, *22*(3), 429–435. https://doi.org/10.1016/0034-4257(87)90094-0

Ribeiro, M., Smith, N. P., Catenacci, F. S., & Cabello, N. B. (2020). Lecythidaceae in Flora do Brasil 2020. *Jardim Botânico do Rio de Janeiro*. http://floradobrasil.jbrj.gov.br/reflora/floradobrasil/FB23424. Accessed 14 June 2021

Richter, H. G., Tomaselli, I., & Moreschi, J. C. (1974). Estudo tecnológico do Guapuruvu (Schizolobium parahyba). *FLORESTA*, *5*(1), 26–30. https://doi.org/10.5380/rf.v5i1.5781

Rodal, M. J. N. ., Sampaio, E. V. S. B., & Figueiredo, M. A. (2013). *Manual sobre métodos de estudo florístico e fitossociológico: Ecossistema Caatinga*. *Sociedade Botânica do Brasil - SBB*. Brasília: SBB.

Romão, M. V. V., & Mansano, V. F. (2020). Schizolobium in Flora do Brasil 2020. *Jardim Botânico do Rio de Janeiro*. http://floradobrasil.jbrj.gov.br/reflora/floradobrasil/FB23143. Accessed 14 June 2021

Rondeaux, G., Steven, M., & Baret, F. (1996). Optimization of soil-adjusted vegetation indices. *Remote Sensing of Environment*, *55*(2), 95–107. https://doi.org/10.1016/0034-4257(95)00186-7

Salomão, R. de P. (2009). Densidade, estrutura e distribuição espacial de castanheira-do-brasil (Bertholletia excelsa H. & B.) em dois platôs de floresta ombrófila densa na Amazônia setentrional brasileira. *Ciências Naturais*, *4*(1), 11–25. http://scielo.iec.gov.br/pdf/bmpegcn/v4n1/v4n1a02.pdf

Sánchez-Azofeifa, G. A., Castro, K., Wright, S. J., Gamon, J., Kalacska, M., Rivard, B., et al. (2009). Differences in leaf traits, leaf internal structure, and spectral reflectance between two communities of lianas and trees: Implications for remote sensing in tropical environments. *Remote Sensing of Environment*, *113*(10), 2076–2088. https://doi.org/10.1016/j.rse.2009.05.013

Silva, C. A. C. P., Silva-Junior, C. A. da, Shiratsuchi, L. S., Lima, M., Rossi, F. S., & Santos, R. C. (2019). Discriminação hiperespectral de mudas de Eucaliptus urophylla x Eucaliptus camaldulensis (VM-01) em condição de deficiência e toxicidade de boro. In *Anais do XIX Simpósio Brasileiro de Sensoriamento Remoto*. Santos: INPE. https://doi.org/10.13140/RG.2.2.28177.07527

Silva Junior, C. A. da, Nanni, M. R., Shakir, M., Teodoro, P. E., de Oliveira-Júnior, J. F., Cezar, E., et al. (2018). Soybean varieties discrimination using non-imaging hyperspectral sensor. *Infrared Physics &Technology*, *89*, 338–350. https://doi.org/10.1016/j.infrared.2018.01.027

Silva Junior, C. A. da, Teodoro, L. P. R., Teodoro, P. E., Baio, F. H. R., de Andrea Pantaleão, A., Capristo-Silva, G. F., et al. (2020). Simulating multispectral MSI bandsets (Sentinel-2) from hyperspectral observations via spectroradiometer for identifying soybean cultivars. *Remote Sensing Applications: Society and Environment*, *19*, 100328. https://doi.org/10.1016/j.rsase.2020.100328

Sims, D. A., & Gamon, J. A. (2002). Relationships between leaf pigment content and spectral reflectance across a wide range of species, leaf structures and developmental stages. *Remote Sensing of Environment*, *81*(2–3), 337–354. https://doi.org/10.1016/S0034-4257(02)00010-X

Souza, C. R. de, Azevedo, C. P. de, Rossi, L. M. B., & Lima, R. M. B. de. (2008). *Castanha-do-Brasil (Bertholletia excelsa Humb & Bonpl.)*. Manaus: Embrapa Amazônia Ocidental.

Steven, M. D. (1998). The Sensitivity of the OSAVI Vegetation Index to Observational Parameters. *Remote Sensing of Environment*, *63*(1), 49–60. https://doi.org/https://doi.org/10.1016/S0034-4257(97)00114-4

Ter Steege, H., Mota de Oliveira, S., Pitman, N. C. A., Sabatier, D., Antonelli, A., Guevara Andino, J. E., et al. (2019). Towards a dynamic list of Amazonian tree species. *Scientific Reports*, *9*(1), 1–5. https://doi.org/10.1038/s41598-019-40101-y

Ter Steege, H., Pitman, N. C. A., Sabatier, D., Baraloto, C., Salomão, R. P., Guevara, J. E., et al. (2013). Hyperdominance in the Amazonian tree flora. *Science*, *342*(6156). https://doi.org/10.1126/science.1243092

Ter Steege, H., Vaessen, R. W., Cárdenas-López, D., Sabatier, D., Antonelli, A., De Oliveira, S. M., et al. (2016). The discovery of the Amazonian tree flora with an updated checklist of all known tree taxa. *Scientific Reports*, *6*, 1–15.

https://doi.org/10.1038/srep29549

Thomas, W. W., Forzza, R. C., Michelangeli, F. A., Giulietti, A. M., & Leitman, P. M. (2012). Large-scale monographs and floras: The sum of local floristic research. *Plant Ecology and Diversity*, *5*(2), 217–223. https://doi.org/10.1080/17550874.2011.622306

Torres, F. E., Teodoro, P. E., Gomes, A. C., Hernandes, F. B., de Lima Fernandes, R., & Ribeiro, L. P. (2015). Adaptability, agronomic performance and genetic divergence of castor genotypes grown in the Cerrado-Pantanal ecotone. *Revista de Ciências Agrarias - Amazon Journal of Agricultural and Environmental Sciences*, *58*(1), 1–5. https://doi.org/10.4322/rca.1700

Vaglio Laurin, G., Cheung-Wai Chan, J., Chen, Q., Lindsell, J. A., Coomes, D. A., Guerriero, L., et al. (2014). Biodiversity mapping in a tropical West African forest with airborne hyperspectral data. *PLoS ONE*, *9*(6). https://doi.org/10.1371/journal.pone.0097910

Vaiphasa, C., Skidmore, A. K., de Boer, W. F., & Vaiphasa, T. (2007). A hyperspectral band selector for plant species discrimination. *ISPRS Journal of Photogrammetry and Remote Sensing*, *62*(3), 225–235. https://doi.org/10.1016/j.isprsjprs.2007.05.006

Vianna, S. A. (2020). Euterpe in Flora do Brasil 2020. *Jardim Botânico do Rio de Janeiro*. http://floradobrasil.jbrj.gov.br/reflora/floradobrasil/FB15713. Accessed 14 June 2021

Ward, J. H. (1963). Hierarchical Grouping to Optimize an Objective Function. *Journal of the American Statistical Association*, *58*(301), 236–244. https://doi.org/10.1080/01621459.1963.10500845

Watt, A. S. (1947). Pattern and Process in the Plant Community. *The Journal of Ecology*, *35*(1/2), 1. https://doi.org/10.2307/2256497

Wu, J., Chavana-Bryant, C., Prohaska, N., Serbin, S. P., Guan, K., Albert, L. P., et al. (2017). Convergence in relationships between leaf traits, spectra and age across diverse canopy environments and two contrasting tropical forests. *New Phytologist*, *214*(3), 1033–1048. https://doi.org/10.1111/nph.14051

CHAPTER II.

CO_2FLUX MODEL ASSESSMENT AND COMPARISON FROM AIRBORNE HYPERSPECTRAL SENSOR TO ORBITAL MULTISPECTRAL IMAGERY

The present manuscript will follow the standards adopted by the journal Remote Sensing of Environment, to which the present work will be submitted.

CHAPTER II. CO_2FLUX MODEL ASSESSMENT AND COMPARISON FROM AIRBORNE HYPERSPECTRAL SENSOR TO ORBITAL MULTISPECTRAL IMAGERY

ABSTRACT

In environmental research, remote sensing techniques are mostly based on orbital data, which is characterized by limited acquisition, besides poor spectral and spatial resolutions. This reflects on carbon dynamics, were orbital remote sensing bears devoted sensor systems for CO_2 monitoring, even though carbon observations are performed with natural resources systems, as Landsat mission, supported by spectral models as CO_2Flux index adapted to multispectral imagery. In this study, this adaptation on Landsat-8, Sentinel-2 and PlanetScope were compared to hyperspectral response of AisaFENIX, based on the same region of interest (ROI) on southern Amazon surveys. After atmospherically correction and radiometric calibration, the scenes were resampled to 30 meters of spatial resolution, seeking for a parametrized comparison of CO_2Flux index, as well as NDVI and PRI given that are formerly indices for CO_2Flux index. From it, analysis of variance was applied to statistically compare indices results among imagery systems and different land uses in the ROI. The results propose a lower reliance of PRI in CO_2Flux index, and hence a greater correlation to NDVI. Seeing the relation among sensors, forest areas had statistical difference in entire comparison scenarios. Still, the anthropized land uses of bare soil and pasture had no statistical difference between Sentinel-2 and AisaFENIX suggesting this multispectral imagery as a feasible source for carbon dynamics assessment. A temporal dynamic assessment could improve these results, where both base indices for CO_2Flux index are related to canopy water content.

Keywords: carbon dynamics; hyperspectral imagery; orbital remote sensing; Brazilian Amazon; CO_2Flux index.

1.Introduction

The global warming (Liu et al., 2020; Noon et al., 2021), human overpopulation (Gambo et al., 2021; Wang and Chen, 2016) and the increase in greenhouse gas concentrations (Ma et al., 2021) have been the subject of studies using remote sensing (RS) techniques. RS has always turned to environmental concerns, especially in land use and land change (LULC) parsing.

Mostly widespread on LULC research, orbital remote sensing data is characterized by limited acquisition, since is generated in a specific time interval around midday, in addition to the presence of clouds, which cover the surface, and involves data missing (Sims et al., 2005). Beyond, most part of sensors on orbital platforms are multispectral, which means poorer spectral resolution, and therefore data restraint (Ponzoni and Shimabukuro, 2009).

Orbital remote sensing bears devoted sensor systems for CO2 monitoring, and assess different scenarios, for instance quantifying power plants emission (Nassar et al., 2021; Ohyama et al., 2021), urban emissions (Lei et al., 2021), wildfire emissions (Guo et al., 2017) and the related measure of solar-induced chlorophyll fluorescence (Du et al., 2018; Li et al., 2021). However, recurrent observing systems as Landsat (Fernandez et al., 2021), Sentinel-2 (Souza et al., 2021) and PlanetScope (Chen et al., 2019) affords reasonable data for modelling or assessing CO2 dynamics (Lees et al., 2018).

In CO2 regard, CO2Flux uptake model (Rahman et al., 2001) aims to parameterizes the photosynthetic flux, originally, of boreal forest stands, taking base on the light use efficiency (LUE). In turn, LUE is related to the fraction of photosynthetically active radiation absorbed by green biomass (fAPAR), i. e. canopy photosynthetic capacity (Garbulsky et al., 2011; Migliavacca et al., 2011; Peñuelas and Inoue, 2000).

Understanding the CO2flux uptake index depends on the associated indices rely on two spectral models. On one hand, the Normalized Difference Vegetation Index (NDVI) expresses the presence or the absence of vegetation and when it comes to vegetation, the type (e. g. forest, soybean, pasture) and its greenness (Rouse J. W. et al., 1974). On the other hand, the Photochemical Reflectance Index (PRI) is related to light use efficiency (LUE) of photosynthetically active vegetation (that is, in visible spectral range) based on hyperspectral data from AVIRIS (Gamon et al., 1997, 1992). Assuming multispectral imagery, PRI and its scaled version (sPRI) data has higher correlation to LUE using MODIS band 13 (662 – 672 nm), using backscattered images (Drolet et al., 2005).

The applicability of CO2Flux uptake model (Rahman et al., 2001) by foundation is based on hyperspectral data of AVIRIS (Airborne Visible/Infrared Imaging Spectrometer), which qualify airborne sensor Specim® AisaFENIX

(SPECIM, 2020). Although, this airborne dataset (in forestry research) sticks to low temporal resolution and availability, hampering the CO2 emission and absorption assessment with this dataset. Even, CO2 surveys are characterized by requiring tuned models to the type of environment (Barnes et al., 2021).

Albeit CO2Flux index (Rahman et al., 2001) formerly based on hyperspectral data, in several studies CO2Flux uptake was assessed by adapting PRI to multispectral imagery, by carrying out this index with blue and green bands, in place of 531 nm and 570 nm, respectively (Cerqueira and Washington Franca-Rocha, 2007; Correia Filho et al., 2021; do Nascimento Lopes et al., 2019; Fernandez et al., 2020; Polonio, 2015; Santos, 2017; Silva Junior et al., 2019; Souza et al., 2021). Even, drought condition affects PRI results in CO2Flux estimation (Inoue et al., 2008).

Towards assert this adapted version, a valuation of CO2Flux index with hyperspectral dataset could reach orbital multispectral imagery systems. Turning to Amazon and using OLI / Landsat-8 multispectral data, CO2Flux values in this LULC patterns varies from 0.48 to -0.09 μmol m^{-2} s^{-1} (Silva Junior et al., 2019).

In this paper, were compared CO2Flux index applied on four imagery systems, in which its scenes in the same ROI (region of interest). This study site affords three different land uses, which are native forest, bare soil and pasture. The contentious applicability of Rahman's model based on multispectral imagery will be discussed with the observation of an imaged Amazon Forest area in northern Mato Grosso state, in Brazil.

2.Materials and methods

2.1 Study site

This research was based on a Specim® AisaFENIX image captured on Alta Floresta city (Latitude 09º52'32"S and Longitude 56º05'10"W, altitude of 283 meters), on northern Mato Grosso state and southern Amazon biome. With an average annual daily temperature of 26,4°C, is characterized by two well-defined climate seasons with high temperatures, the rainy and the dry season, classified as Aw according to Köppen-Geiger Climate Classification, and an average annual rainfall of 2281 milimeters.

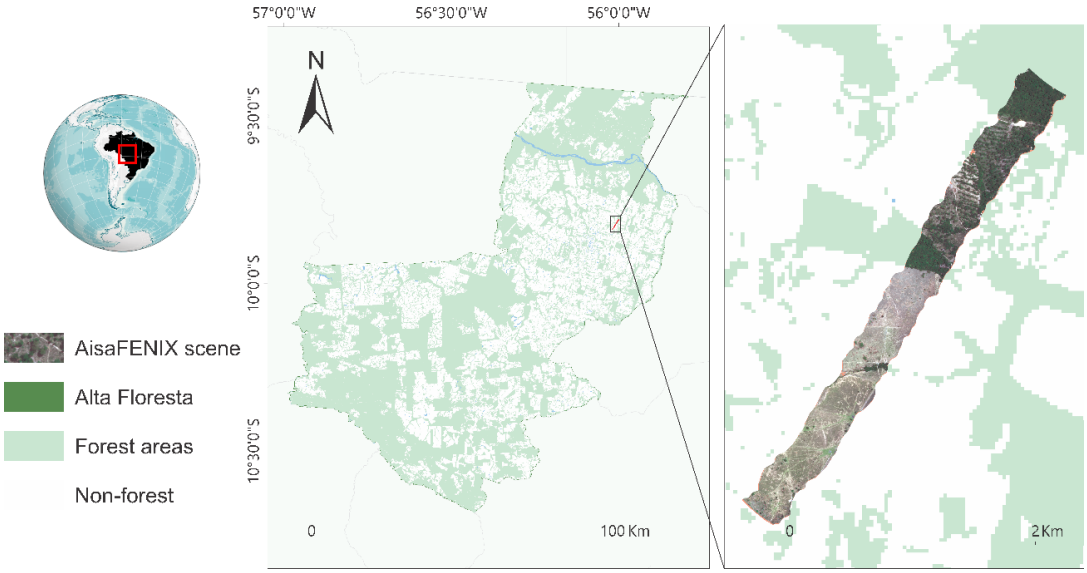

Fig. 1. Imaged area in Alta Floresta, southern Brazilian Amazon and forest areas in the city, Northern Mato Grosso state.

The imaged area was taken in Alta Floresta urban zone purlieu. It is worth pointing out this area features native forest area, pasture area and bare soil, which have different CO_2 emission patterns, within distinct land uses means different carbon gains or losses (Ostle et al., 2009).

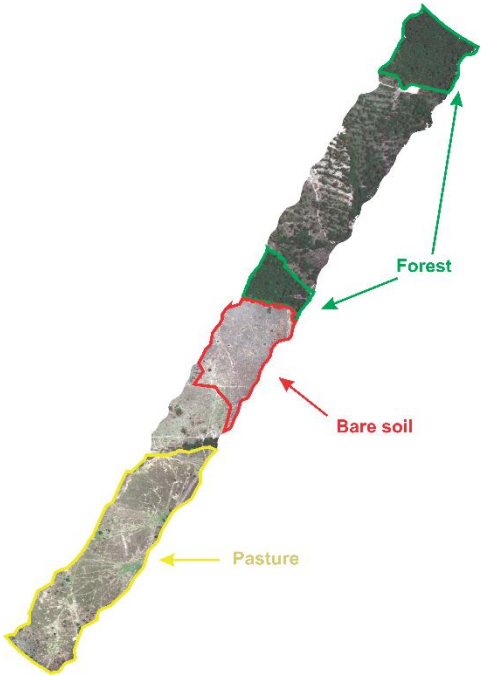

Fig. 2. Regions of interest, classified as forest (green), bare soi (red) and pasture (yellow) areas in the study site.

2.2. Data procurement and image pre-processing

2.2.1. Hyperspectral image

As abovementioned, the hyperspectral image (HSI) is based on Specim® AisaFENIX (SPECIM, 2020), a push broom imaging hyperspectral spectrometer, which covers a spectral range from 380 nm to 2500 nm, i. e., comprise visible, near infrared and short wave infrared. Data collection was conducted on 9th October 2017, on board of an aircraft. Thereafter, the radiometric correction of image was carried out using CaliGeo Pro software, designed by Specim.

Table 1

Detail of AisaFENIX system and data acquisition traits.

	VNIR[1]	**SWIR**[2]
Spectral range	380 ~ 970 nm	970 ~ 2500 nm
Spectral bands	344	275
Detector	Complementary metal-oxide-semiconductor (CMOS)	Mercury Cadmium Telluride (MCT) cooled detector
Spectral resolution	3.5 nm	12 nm
Field of View	32.3°	
Focal aperture	F/2.4	
Radiometric resolution	16 bits	
Imaging speed	130 frames per second	
Spatial resolution	0.65 m (at 600 m of altitude)	

[1]VNIR: Visible and Near-Infrared; [2]SWIR: Short-Wave infrared.

2.2.2. *Orbital data*

High temporal resolution from orbital datasets improves data acquisition, making remote sensing approaches eligible in environmental assessments. Working on open access imagery, were chosen OLI/Landsat-8, MSI/Sentinel-2 and PlanetScope data. Orbital data chosen were based on the nearest day of acquisition related to HSI data collection.

Data from Landsat-8 has medium spatial resolution varying from 15 to 100 meters, and as a free-access data has a plenty use in remote sensing. OLI (Operational Land Imager) sensor have nine spectral (Table 2) bands ranging from visible electromagnetic spectrum to short-wave infrared ("Landsat 8 | U.S. Geological Survey," n.d.). In this study, were applied the required bands for NDVI

(band 4 for red and band 5 for near infrared) and the adapted PRI (band 2 for blue and band 3 for green), which has 30 meters of spatial resolution.

Table 2

OLI/Landsat-8 bands characterization

Band name	Description	Spectral range (nm)
B1	**Coastal/Aerosol**	433 ~ 453
B2	**Blue**	450 ~ 515
B3	**Green**	525 ~ 600
B4	**Red**	630 ~ 680
B5	**Near Infrared**	845 ~ 885
B6	**SWIR 1**	1560 ~ 1660
B7	**SWIR 2**	2100 ~ 2300
B8	**Panchromatic**	500 ~ 680
B9	**Cirrus**	1360 ~ 1390

In order to assess free-access orbital data, MSI sensor on board both Sentinel-2 mission satellites fits in this criterion. This imagery has medium spatial resolution ranging from 10 to 60 meters, over 13 spectral bands (Table 3) from visible to short-wave infrared, as seen on OLI/Landsat-8 system ("MSI Instrument – Sentinel-2 MSI Technical Guide – Sentinel Online - Sentinel Online," n.d.). Here, the NDVI is based on bands 8 (Near infrared) and 4 (Red), while adapted PRI is calculated using bands 2 (Blue) and 3 (Green), where these bands have spatial resolution of 10 meters.

Table 3

MSI/Sentinel-2 bands characterization

Band name	Description	Spectral range (nm)
B01	**Aerosols**	421.7 ~ 463.7
B02	**Blue**	426.4 ~ 558.4
B03	**Green**	523.8 ~ 595.8
B04	**Red**	633.6 ~ 695.6
B05	**Red edge 1**	689.1 ~ 719.1
B06	**Red edge 2**	725.5 ~ 755.5
B07	**Red edge 3**	762.8 ~ 802.8

B08	**Near infrared**	726.8 ~ 938.8
B08a	**Red edge 4**	843.7 ~ 885.7
B09	**Water vapor**	925.1 ~ 965.1
B10	**Cirrus**	1342.5 ~1404.5
B11	**SWIR 1**	1522.7 ~ 1704.7
B12	**SWIR 2**	2027.4 ~ 2377.4

In detail, the orbital data from Landsat-8 system were obtained on October 6th 2017. The study site was completely covered by one scene from this imagery. Regarding to Sentinel-2, it took two scenes to cover the entire study site, based on October 14th 2017. Last, PlanetScope image was acquired through Google Earth Engine, based on October 7th 2017 survey. The orbital data was corrected, that is scattering effect minimizing and radiometric calibration was carried out to correct the images.

Table 4

Detail of scenes from orbital platforms.

Imagery	Scene
OLI/Landsat-8	LANDSAT/LC08/C01/T1_RT_TOA/LC08_227067_20171006
MSI/Sentinel-2	20171014T140051_20171014T140051_T21LWK
	20171014T140051_20171014T140051_T21LXK
PlanetScope	Acquisition through Google Earth Engine

2.3. Data processing

After acquisition (with atmospheric and shape correction), the AisaFENIX scene and the orbital data were handled on ArcMap 10.8 software. The tool "Resample" (Fig. 3) was applied on data tuned to nearest resampling, in order to equalize spatial resolution among the different databases. Thus, AisaFENIX, PlanetScope and MSI/Sentinel-2 data were lowered to 30 meters of spatial resolution.

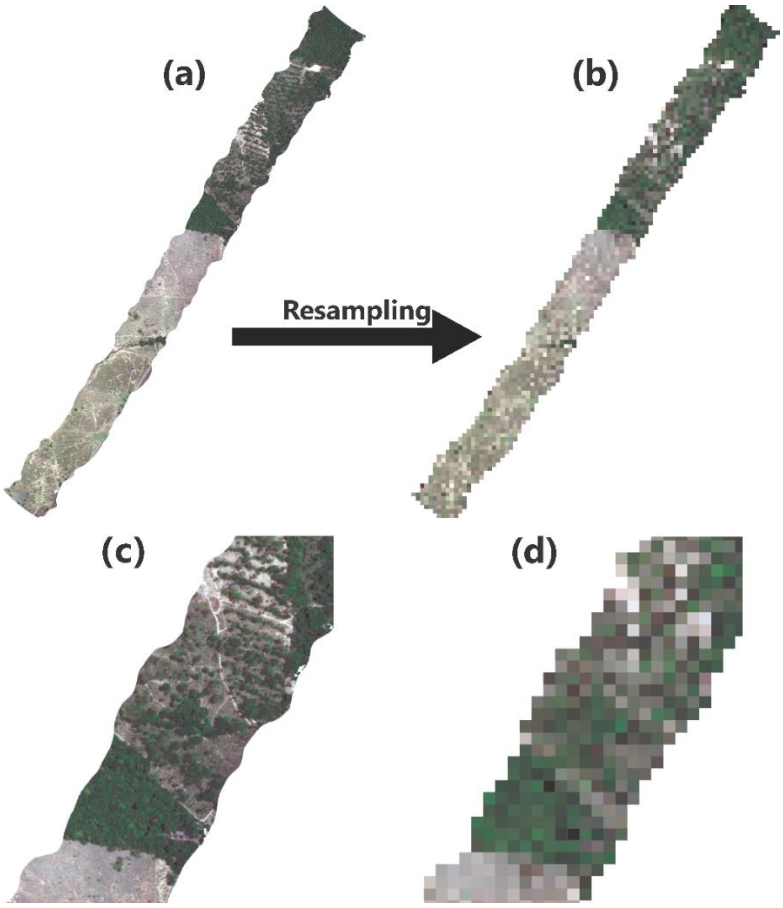

Fig. 3. Resample tool (ArcMap 10.8) processing on original (a) AisaFENIX scene to resampled (b) scene, with RGB composition on bands 42, 26 and 12. Scene detail from original (c) and resampled (d) image.

In order to take only the ROI (Region of interest), "Extract by mask" tool on ArcMap 10.8 was used. After that, were calculated the indices on which CO_2Flux uptake model is based, namely NDVI, PRI (and its scaled version) and CO_2Flux index itself through QGIS3 software, using the tool "Band Math".

$$NDVI = \frac{\rho_{NIR} - \rho_{RED}}{\rho_{NIR} + \rho_{RED}} \quad (1)$$

$$PRI = \frac{\rho_{531nm} - \rho_{570nm}}{\rho_{531nm} + \rho_{570nm}} \quad (2)$$

$$sPRI = \frac{PRI + 1}{2} \quad (3)$$

$$CO_2Flux = sPRI \times NDVI \quad (4)$$

The selected bands to replace ρ531nm and ρ570 nm on orbital datasets were blue and green bands respectively, as aforementioned in referenced research. In turn, the AisaFENIX bands used in the VI's calculation were the closer to the reference on models, 62 for ρ_{NIR} and 42 for ρ_{RED} in NDVI equation, and bands 23 and 29 for ρ531nm and ρ570 nm in PRI equation.

2.4. Statistical approach

For each variable evaluated, analysis of variance was performed considering an entirely randomized design with 10 repetitions in a 4x3 factorial scheme (four sensors vs three land use and land cover). Subsequently, Tukey's test was applied for multiple comparisons of means. In all cases, a 5% significance level was adopted.

3. Results

3.1. CO_2Flux index

Initially, the spectral data from airborne and orbital systems were processed and undergone on index calculation. From this approach, the band math was carried out with NDVI (Fig. 4), PRI (Fig. 5) and mainly with CO_2Flux (Fig. 6) in the ROI. The spectral profile along the scene from this calculation is presented on Supplementary Material.

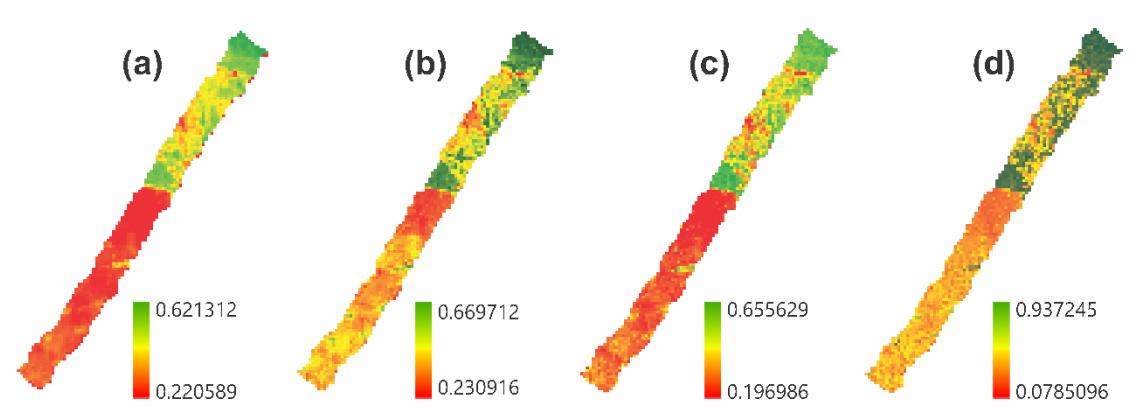

Fig. 4. Normalized Difference Vegetation Index (NDVI) results for OLI/Landsat-8 (a), MSI/Sentinel-2 (b), PlanetScope (c) and AisaFENIX data.

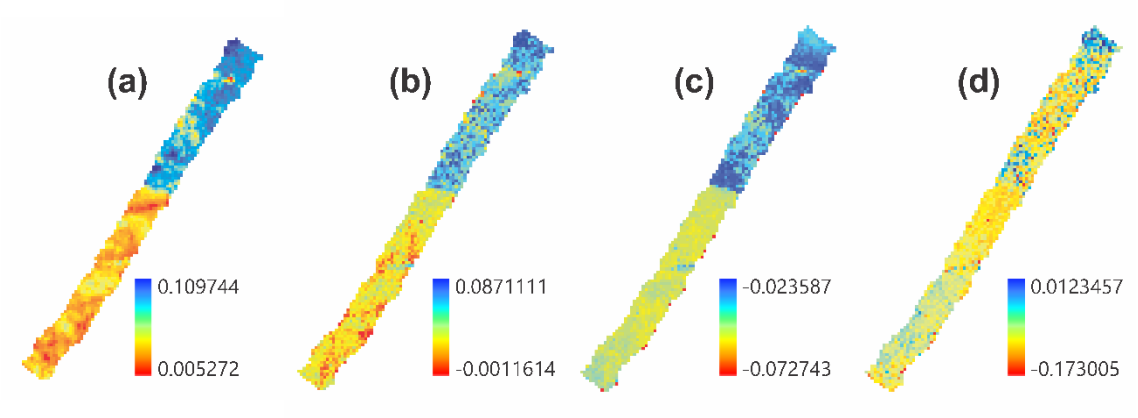

Fig. 5. Photochemical Reflectance Index (PRI) results for OLI/Landsat-8 (a), MSI/Sentinel-2 (b), PlanetScope (c) and AisaFENIX data.

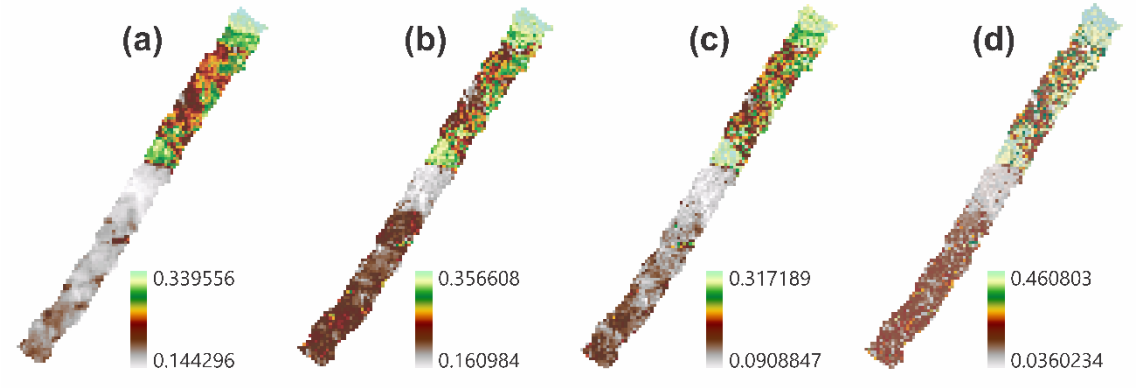

Fig. 6. CO_2Flux uptake index results for OLI/Landsat-8 (a), MSI/Sentinel-2 (b), PlanetScope (c) and AisaFENIX data.

By using 3D analyst on ArcMap 10.8, were generated the profile graphs based on a north-south transect aligned to the scene, described in the OLI/Landsat-8 scene with RGB true color composition on Fig. 7. It's worth pointing those lower values on horizontal axis concern forest land use, while higher values are about bare soil, and beyond for pasture.

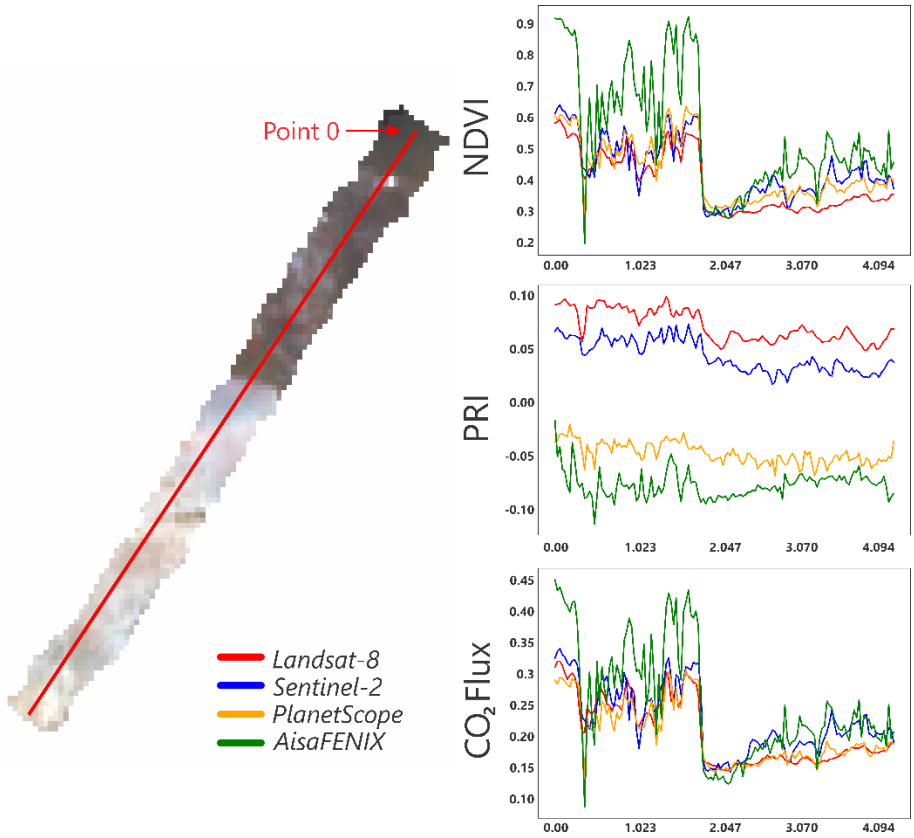

Fig. 7. Transect on the OLI/Landsat-8 scene (left) and NDVI, PRI and CO2Flux spectral profiles (right) based on the transect. Horizontal axis refers to the spatial variation over the transect line (Kilometers), while vertical axis represents the index value.

3.2. Statistical approach

There was significant interaction on sensors and Land Uses and Land Cover (LULC) comparisons for all evaluated variables (Figure 8). This indicates that there is differential behavior of the sensors along each LULC and back again. In order to appreciate Fig. 8 results, there is no statistical difference when comparing sensors (lowercase) or LULC (uppercase) with same letter.

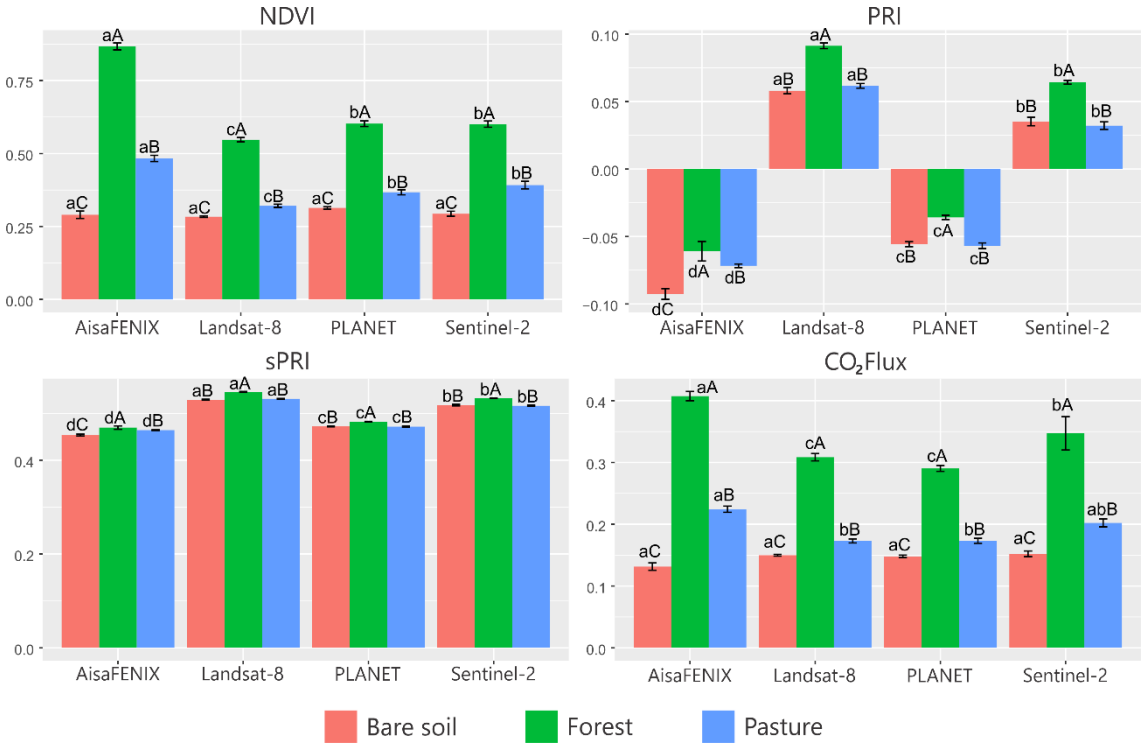

Fig. 8. Significant interaction among sensors versus LULC for the vegetation indices NDVI, PRI, sPRI and CO_2Flux. Uppercase letters express statistical similarity or difference on by comparing LULC for the same sensor, and lowercase letters express statistical similarity or difference on the same LULC for different sensors.

For NDVI (Fig. 9) and CO_2Flux (Fig. 10), bare soil had no statistical difference among sensors. However, the AisaFENIX sensor had the highest NDVI averages in comparison to multispectral sensors turning to forest and pasture. Also, it is observed that the forest presented the highest NDVI averages in relation to other LULC, regardless of the sensor as expected.

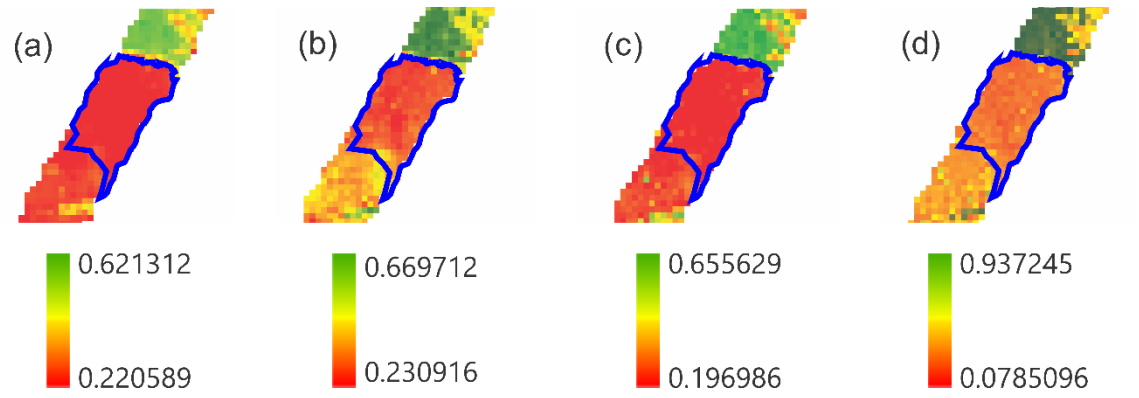

Fig. 9. NDVI on bare soil area (blue polygon) based on Landsat-8 (a), Sentinel-2 (b), PLANET (c) and AisaFENIX (d) scenes.

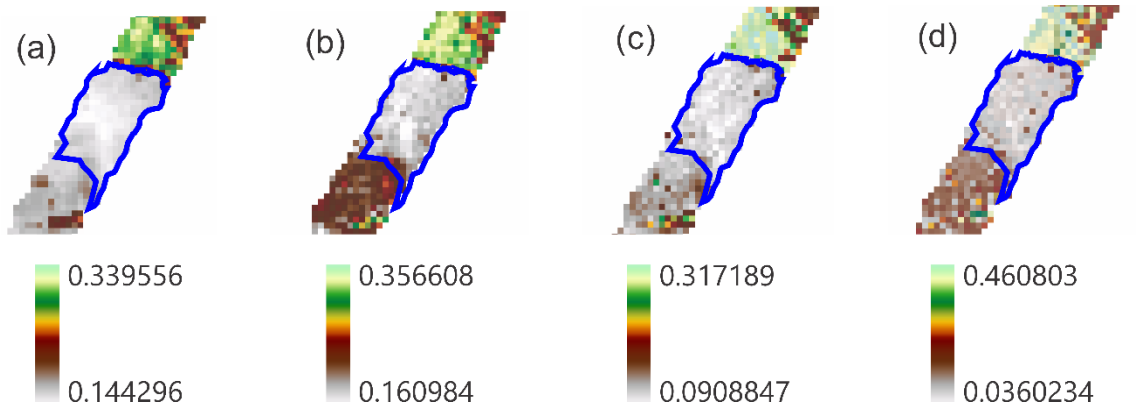

Fig. 10. CO_2Flux index on bare soil area (blue polygon) based on Landsat-8 (a), Sentinel-2 (b), PLANET (c) and AisaFENIX (d) scenes.

Regarding to PRI or sPRI, were spotted higher mean values on Landsat-8 dataset compared to other sensors. Furthermore, among LULC types, forest presented the highest mean values of PRI and sPRI. Despite this, sPRI values across the entire dataset were close to zero, irrespective of LULC and sensor.

Concerning CO_2Flux, the AisaFENIX sensor reached the highest averages in relation to the others for forest and pasture, despite pasture did not differ statistically by comparing AisaFENIX to Sentinel-2 (Fig. 11). As with the other vegetation indices, forest presented the highest averages by comparing to other LULC, regardless of the sensor.

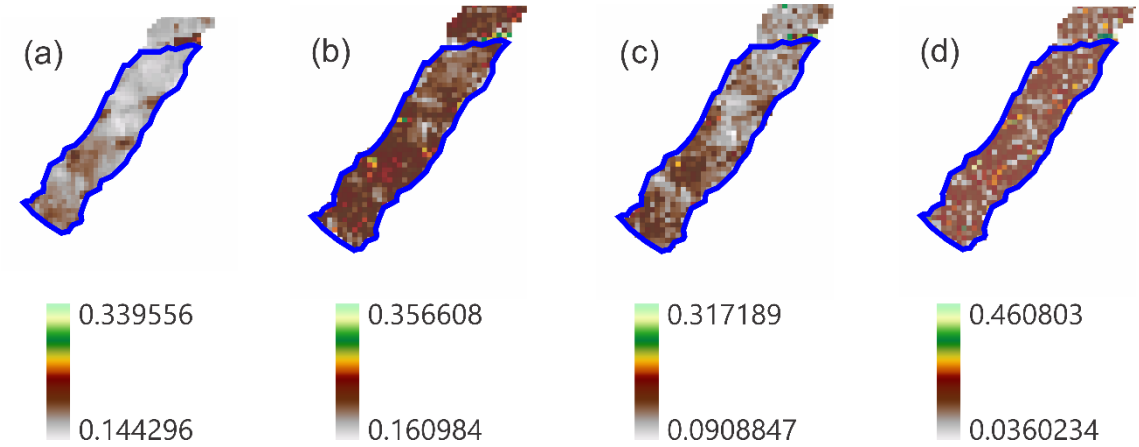

Fig. 11. CO_2Flux index on pasture area (blue polygon) based on Landsat-8 (a), Sentinel-2 (b), PLANET (c) and AisaFENIX (d) scenes.

4. Discussion

The atmospheric carbon and related uptake and emission phenomena assessment through remote sensing techniques can be grounded on net ecosystem exchange (NEE) or more seldom on CO_2Flux uptake (Rahman et al., 2001)

estimations, for instance this paper. In the first case, collateral information and rugged computational tools and techniques are required (Zhang et al., 2021). On the other hand, CO_2Flux uptake take merely remote sensing data, what prompted this and the abovementioned research.

Regarding to PRI, the substantial difference in this VI (and on it scaled version sPRI) among sensors was evident, owing to different blue and green bands in multispectral and hyperspectral bands. This difference is greater on hyper versus multispectral comparison, where both narrow PRI reference bands are in the blue range in the three orbital sensors considered in this study.

The comparison between OLI and MSI on savanna areas and using the aforementioned resampling reached root mean square difference of 0.0314 (Zhang et al., 2018), what could be similarly seen on this work, despite being an evergreen forest area. Herein, NDVI values were statistically distinct between OLI to MSI comparison, both in forest and pasture LULC, which most resemble the savanna.

From the analysis of variance illustrated on Fig. 8, we observed that comparison among sensors and LULC were similar between NDVI and CO_2Flux, suggesting that PRI does not contribute significantly to CO_2Flux in these conditions. Nevertheless, it was also thought that environmental conditions related to drought would affect PRI performance (Hwang et al., 2017), as in this estimation model (Inoue et al., 2008), suggesting further assessment on CO_2Flux uptake model considering temporal variations related to drought and rainfall seasonality, since the performance of carbon sinks is related to canopy water content (Asner et al., 2016).

The presence of NDVI on CO_2Flux index rely on biomass measurement and its greenness (Rahman et al., 2001), as NDVI performs best in leaf biomass estimation, where PlanetScope and Sentinel-2 data has been assessed as good predictors of aboveground biomass, which in turn is the greatest carbon pool in trees (Baloloy et al., 2018). In remote sensing, the Gross Primary Production (GPP) is another metric for CO_2 balance, which expresses the uptake via photosynthesis, and is weaklier related to NDVI on LULC with higher NDVI values (Menefee et al., 2020). Herein, higher values of NDVI had lower correlation among datasets specially on forest areas, and except on PlanetScope versus Sentinel-2 comparison, which in

spatial assessment similar results were expected from phenological research work (Cheng et al., 2020).

Atmospheric carbon dioxide uptake assessed through CO_2Flux index provides a metric related to land cover, limited on temporal variability. However, considering land use change is more appropriate in the current scenario for the Amazonian rainforest, taking into account the rainfall seasonality and the climate variations that so greatly affect the carbon uptake capacity of carbon sinks (Asner et al., 2004). This suggests to us that the model is potentially functional when studying spatial-temporal dynamics of this biome.

In a broad observation of multispectral sensors results, MSI/Sentinel-2 has the closer results to AisaFENIX, noting that there is no statistical difference in bare soil and pasture among datasets, by analysis of variance. Despite CO_2Flux with difference among sensors, NDVI had similar difference, what justifies further hyper-multispectral comparison studies, especially in the Amazon biome.

5. Conclusions

We compared the CO_2Flux uptake index among four imagery datasets, demonstrating that this index can be based on open-access orbital multispectral imagery, bearing sufficient data for carbon uptake modelling. The results shown in this paper suggests MSI/Sentinel-2 closer results related to hyperspectral data from AisaFENIX sensor on anthropized areas of bare soil and pasture, with no statistical difference between these sensors. Mainly, the CO2Flux uptake index on multispectral data and in AisaFENIX with results closer to NDVI expresses easily dependent on PRI. Even, the spatial-temporal dynamics of rainfall seasonality relation to CO_2 uptake should be assessed in future research. Furthermore, research applications using CO_2Flux uptake index directly using Sentinel-2 data will be enforceable, especially on LULC similar to pasture and bare soil, as seen in livestock lands.

References

Asner, G.P., Nepstad, D., Cardinot, G., Ray, D., 2004. Drought stress and carbon uptake in an Amazon forest measured with spaceborne imaging spectroscopy. Proc.

Natl. Acad. Sci. 101, 6039–6044. https://doi.org/10.1073/pnas.0400168101

Barnes, M.L., Farella, M.M., Scott, R.L., Moore, D.J.P., Ponce-Campos, G.E., Biederman, J.A., MacBean, N., Litvak, M.E., Breshears, D.D., 2021. Improved dryland carbon flux predictions with explicit consideration of water-carbon coupling. Commun. Earth Environ. 2, 248. https://doi.org/10.1038/s43247-021-00308-2

Cerqueira, D.B. De, Washington Franca-Rocha, 2007. Relação entre tipos de vegetação e fluxo de CO2 no Bioma Caatinga: Estudo de caso em Rio de Contas - Ba, in: Anais XIII Simpósio Brasileiro de Sensoriamento Remoto. pp. 2413–2419.

Chen, Y., Guerschman, J.P., Cheng, Z., Guo, L., 2019. Remote sensing for vegetation monitoring in carbon capture storage regions: A review. Appl. Energy 240, 312–326. https://doi.org/https://doi.org/10.1016/j.apenergy.2019.02.027

Correia Filho, W.L.F., Santiago, D. de B., Oliveira-Júnior, J.F. de, Silva Junior, C.A. da, Oliveira, S.R. da S., Silva, E.B. da, Teodoro, P.E., 2021. Analysis of environmental degradation in Maceió-Alagoas, Brazil via orbital sensors: A proposal for landscape intervention based on urban afforestation. Remote Sens. Appl. Soc. Environ. 24, 100621. https://doi.org/https://doi.org/10.1016/j.rsase.2021.100621

do Nascimento Lopes, E.R., Sousa, J.A.P. De, Souza, J.C. De, Filho, J.L.A., Lourenço, R.W., 2019. Spatial dynamics of Atlantic Forest fragments in a river basin. FLORESTA 50, 1053. https://doi.org/10.5380/rf.v50i1.61076

Drolet, G.G., Huemmrich, K.F., Hall, F.G., Middleton, E.M., Black, T.A., Barr, A.G., Margolis, H.A., 2005. A MODIS-derived photochemical reflectance index to detect inter-annual variations in the photosynthetic light-use efficiency of a boreal deciduous forest. Remote Sens. Environ. 98, 212–224. https://doi.org/https://doi.org/10.1016/j.rse.2005.07.006

Du, S., Liu, L., Liu, X., Zhang, Xiao, Zhang, Xingying, Bi, Y., Zhang, L., 2018. Retrieval of global terrestrial solar-induced chlorophyll fluorescence from TanSat satellite. Sci. Bull. 63, 1502–1512. https://doi.org/https://doi.org/10.1016/j.scib.2018.10.003

Fernandez, H.M., Gomes, C.P., Granja-martins, F.M., 2020. Monitorização por satélite da desflorestação da floresta do Maiombe em Cabinda, Angola nos últimos 33 anos. Rev. GEAMA - Ciências Ambient. e Biotecnol. 6, 81–91.

Fernandez, H.M., Granja-Martins, F.M., Pedras, C.M.G., Fernandes, P., Isidoro, J.M.G.P., 2021. An Assessment of Forest Fires and CO2 Gross Primary Production from 1991 to 2019 in Mação (Portugal). Sustain. . https://doi.org/10.3390/su13115816

Gambo, J., Ahmed Yusuf, Y., Zulhaidi bin Mohd Shafri, H., Salihu Lay, U., Ahmed, A., 2021. A Three Decades Urban Growth Monitoring in Hadejia, Nigeria Using Remote Sensing and Geospatial Techniques. IOP Conf. Ser. Earth Environ. Sci. 620, 12012. https://doi.org/10.1088/1755-1315/620/1/012012

Gamon, J., Serrano, L., Surfus, J.S., 1997. The Photochemical Reflectance Index: An Optical Indicator of Photosynthetic Radiation Use Efficiency across Species, Functional Types, and Nutrient Levels. Oecologia 112, 492–501. https://doi.org/10.1007/s004420050337

Gamon, J.A., Peñuelas, J., Field, C.B., 1992. A narrow-waveband spectral index that tracks diurnal changes in photosynthetic efficiency. Remote Sens. Environ. 41, 35–44. https://doi.org/https://doi.org/10.1016/0034-4257(92)90059-S

Garbulsky, M.F., Peñuelas, J., Gamon, J., Inoue, Y., Filella, I., 2011. The photochemical reflectance index (PRI) and the remote sensing of leaf, canopy and ecosystem radiation use efficiencies: A review and meta-analysis. Remote Sens. Environ. 115, 281–297. https://doi.org/https://doi.org/10.1016/j.rse.2010.08.023

Guo, M., Li, J., Xu, J., Wang, X., He, H., Wu, L., 2017. CO2 emissions from the 2010 Russian wildfires using GOSAT data. Environ. Pollut. 226, 60–68. https://doi.org/https://doi.org/10.1016/j.envpol.2017.04.014

Inoue, Y., Peñuelas, J., Miyata, A., Mano, M., 2008. Normalized difference spectral indices for estimating photosynthetic efficiency and capacity at a canopy scale derived from hyperspectral and CO2 flux measurements in rice. Remote Sens. Environ. 112, 156–172. https://doi.org/https://doi.org/10.1016/j.rse.2007.04.011

Landsat 8 | U.S. Geological Survey [WWW Document], n.d. URL https://www.usgs.gov/landsat-missions/landsat-8 (accessed 1.3.22).

Lees, K.J., Quaife, T., Artz, R.R.E., Khomik, M., Clark, J.M., 2018. Potential for using remote sensing to estimate carbon fluxes across northern peatlands – A review. Sci. Total Environ. 615, 857–874. https://doi.org/https://doi.org/10.1016/j.scitotenv.2017.09.103

Lei, R., Feng, S., Danjou, A., Broquet, G., Wu, D., Lin, J.C., O'Dell, C.W., Lauvaux, T., 2021. Fossil fuel CO2 emissions over metropolitan areas from space: A multi-model analysis of OCO-2 data over Lahore, Pakistan. Remote Sens. Environ. 264, 112625. https://doi.org/https://doi.org/10.1016/j.rse.2021.112625

Li, S., Gao, M., Li, Z.-L., Duan, S., Leng, P., 2021. Uncertainty analysis of SVD-based spaceborne far–red sun-induced chlorophyll fluorescence retrieval using TanSat satellite data. Int. J. Appl. Earth Obs. Geoinf. 103, 102517. https://doi.org/https://doi.org/10.1016/j.jag.2021.102517

Liu, J., Huang, R., Yu, K., Zou, B., 2020. How lime-sand islands in the South China Sea have responded to global warming over the last 30 years: Evidence from satellite remote sensing images. Geomorphology 371, 107423. https://doi.org/https://doi.org/10.1016/j.geomorph.2020.107423

Ma, A., Chen, D., Zhong, Y., Zheng, Z., Zhang, L., 2021. National-scale greenhouse mapping for high spatial resolution remote sensing imagery using a dense object dual-task deep learning framework: A case study of China. ISPRS J. Photogramm. Remote Sens. 181, 279–294. https://doi.org/https://doi.org/10.1016/j.isprsjprs.2021.08.024

Migliavacca, M., Galvagno, M., Cremonese, E., Rossini, M., Meroni, M., Sonnentag, O., Cogliati, S., Manca, G., Diotri, F., Busetto, L., Cescatti, A., Colombo, R., Fava, F., Morra di Cella, U., Pari, E., Siniscalco, C., Richardson, A.D., 2011. Using digital repeat photography and eddy covariance data to model grassland phenology and photosynthetic CO2 uptake. Agric. For. Meteorol. 151, 1325–1337. https://doi.org/https://doi.org/10.1016/j.agrformet.2011.05.012

MSI Instrument – Sentinel-2 MSI Technical Guide – Sentinel Online - Sentinel Online [WWW Document], n.d. URL https://sentinels.copernicus.eu/web/sentinel/technical-guides/sentinel-2-msi/msi-instrument (accessed 1.3.22).

Nassar, R., Mastrogiacomo, J.-P., Bateman-Hemphill, W., McCracken, C., MacDonald, C.G., Hill, T., O'Dell, C.W., Kiel, M., Crisp, D., 2021. Advances in quantifying power plant CO2 emissions with OCO-2. Remote Sens. Environ. 264, 112579. https://doi.org/https://doi.org/10.1016/j.rse.2021.112579

Noon, M.L., Goldstein, A., Ledezma, J.C., Roehrdanz, P.R., Cook-Patton, S.C., Spawn-Lee, S.A., Wright, T.M., Gonzalez-Roglich, M., Hole, D.G., Rockström, J., Turner,

W.R., 2021. Mapping the irrecoverable carbon in Earth's ecosystems. Nat. Sustain. https://doi.org/10.1038/s41893-021-00803-6

Ohyama, H., Shiomi, K., Kikuchi, N., Morino, I., Matsunaga, T., 2021. Quantifying CO2 emissions from a thermal power plant based on CO2 column measurements by portable Fourier transform spectrometers. Remote Sens. Environ. 267, 112714. https://doi.org/https://doi.org/10.1016/j.rse.2021.112714

Ostle, N.J., Levy, P.E., Evans, C.D., Smith, P., 2009. UK land use and soil carbon sequestration. Land Use Policy 26, S274–S283. https://doi.org/https://doi.org/10.1016/j.landusepol.2009.08.006

Peñuelas, J., Inoue, Y., 2000. Reflectance assessment of canopy CO2 uptake. Int. J. Remote Sens. 21, 3353–3356. https://doi.org/10.1080/014311600750019958

Polonio, V.D., 2015. Índices de vegetação na mensuração do estoque de carbono em áreas com cana-de-açúcar. UNESP.

Ponzoni, F.J., Shimabukuro, Y.E., 2009. Sensoriamento remoto no estudo da vegetação. Parêntese Editora, São José dos Campos.

Rahman, A.F., Gamon, J.A., Fuentes, D.A., Roberts, D.A., Prentiss, D., 2001. Modeling spatially distributed ecosystem flux of boreal forest using hyperspectral indices from AVIRIS imagery. J. Geophys. Res. Atmos. 106, 33579–33591. https://doi.org/10.1029/2001jd900157

Rouse J. W., J., Haas, R.H., Schell, J.A., Deering, D.W., 1974. Monitoring Vegetation Systems in the Great Plains with ERTS, in: Proceeding of ERTS-1 Symposium. p. 309.

Santos, C.V.B. dos, 2017. Modelagem espectral para determinação de fluxo de CO_2 em áreas de caatinga preservada e em regeneração cloves. Universidade Estadual de Feira de Santana.

Silva Junior, C.A. da, Costa, G. de M., Rossi, F.S., Vale, J.C.E. do, Lima, R.B. de, Lima, M., Oliveira-Junior, J.F. de, Teodoro, P.E., Santos, R.C., 2019. Remote sensing for updating the boundaries between the brazilian Cerrado-Amazonia biomes. Environ. Sci. Policy 101, 383–392. https://doi.org/10.1016/j.envsci.2019.04.006

Sims, D.A., Rahman, A.F., Cordova, V.D., Baldocchi, D.D., Flanagan, L.B., Goldstein, A.H., Hollinger, D.Y., Misson, L., Monson, R.K., Schmid, H.P., Wofsy, S.C., Xu, L.,

2005. Midday values of gross CO2 flux and light use efficiency during satellite overpasses can be used to directly estimate eight-day mean flux. Agric. For. Meteorol. 131, 1–12. https://doi.org/https://doi.org/10.1016/j.agrformet.2005.04.006

Souza, A.P.D., Teodoro, P.E., Teodoro, L.P.R., Taveira, A.C., de Oliveira-Júnior, J.F., Della-Silva, J.L., Baio, F.H.R., Lima, M., da Silva Junior, C.A., 2021. Application of remote sensing in environmental impact assessment: a case study of dam rupture in Brumadinho, Minas Gerais, Brazil. Environ. Monit. Assess. 193, 606. https://doi.org/10.1007/s10661-021-09417-z

SPECIM, 2020. AisaFENIX - Specim [WWW Document]. AisaFENIX. URL https://www.specim.fi/products/aisafenix/ (accessed 3.29.21).

Wang, L., Chen, L., 2016. Spatiotemporal dataset on Chinese population distribution and its driving factors from 1949 to 2013. Sci. Data 3, 160047. https://doi.org/10.1038/sdata.2016.47

Zhang, C., Brodylo, D., Sirianni, M.J., Li, T., Comas, X., Douglas, T.A., Starr, G., 2021. Mapping CO2 fluxes of cypress swamp and marshes in the Greater Everglades using eddy covariance measurements and Landsat data. Remote Sens. Environ. 262, 112523. https://doi.org/https://doi.org/10.1016/j.rse.2021.112523

Zhang, H.K., Roy, D.P., Yan, L., Li, Z., Huang, H., Vermote, E., Skakun, S., Roger, J.-C., 2018. Characterization of Sentinel-2A and Landsat-8 top of atmosphere, surface, and nadir BRDF adjusted reflectance and NDVI differences. Remote Sens. Environ. 215, 482–494. https://doi.org/https://doi.org/10.1016/j.rse.2018.04.031